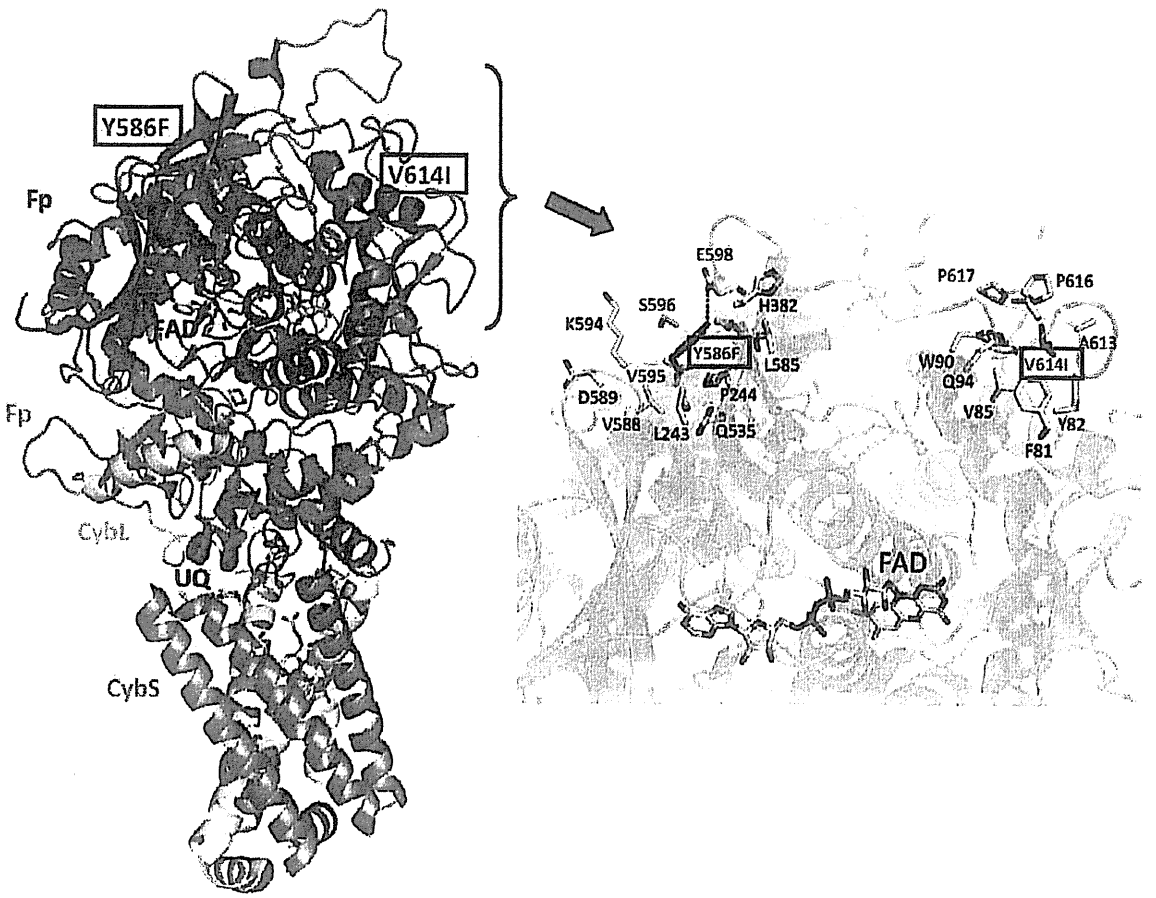
Y586F
V614I
Fp
FAD
Fp
CybL
UQ
CybS
E598
S596
H382
K594
Y586F
L585
V595
P244
D589
V588
L243
Q535
P617
P616
A613
W90
V614I
Q94
V85
Y82
F81
FAD

Figure 10

⌘ *Author's Choice*

THE JOURNAL OF BIOLOGICAL CHEMISTRY VOL. 287, NO. 20, pp. 16379–16389, May 11, 2012

Muscle-specific Knock-out of NUAK Family SNF1-like Kinase 1 (NUAK1) Prevents High Fat Diet-induced Glucose Intolerance*[S]

Received for publication, September 13, 2011, and in revised form, March 9, 2012 Published, JBC Papers in Press, March 14, 2012, DOI 10.1074/jbc.M111.302687

Fumika Inazuka[‡§], Naoyuki Sugiyama[¶], Masaru Tomita[¶], Takaya Abe[‖], Go Shioi[‖], and Hiroyasu Esumi[‡§1]

From the [‡]Department of Integrated Biosciences, Graduate School of Frontier Sciences, The University of Tokyo, Kashiwa 277-8561, Japan, the [§]Cancer Physiology Project, Research Center for Innovative Oncology, National Cancer Center Hospital East, Kashiwa 277-8577, Japan, the [¶]Institute for Advanced Biosciences, Keio University, Tsuruoka 997-0017, Japan, and the [‖]Laboratory for Animal Resources and Genetic Engineering, RIKEN Center for Developmental Biology, Kobe, 650-0047, Japan

Background: The physiological roles of NUAK1 are poorly understood because of embryonic lethality in NUAK1 null mice.
Results: Negative feedback regulation of insulin signaling was abrogated in skeletal muscle of muscle-specific NUAK1 knock-out mice.
Conclusion: NUAK1 controls glucose metabolism through negative regulation of insulin signal transduction in skeletal muscle.
Significance: This is the first report of a physiological role of NUAK1 in adult tissues.

NUAK1 is a member of the AMP-activated protein kinase-related kinase family. Recent studies have shown that NUAK1 is involved in cellular senescence and motility in epithelial cells and fibroblasts. However, the physiological roles of NUAK1 are poorly understood because of embryonic lethality in NUAK1 null mice. The purpose of this study was to elucidate the roles of NUAK1 in adult tissues. We determined the tissue distribution of NUAK1 and generated muscle-specific NUAK1 knock-out (MNUAK1KO) mice. For phenotypic analysis, whole body glucose homeostasis and muscle glucose metabolism were examined. Quantitative phosphoproteome analysis of soleus muscle was performed to understand the molecular mechanisms underlying the knock-out phenotype. Nuak1 mRNA was preferentially expressed in highly oxidative tissues such as brain, heart, and soleus muscle. On a high fat diet, MNUAK1KO mice had a lower fasting blood glucose level, greater glucose tolerance, higher insulin sensitivity, and higher concentration of muscle glycogen than control mice. Phosphoproteome analysis revealed that phosphorylation of IRS1 Ser-1097 was markedly decreased in NUAK1-deficient muscle. Consistent with this, insulin signaling was enhanced in the soleus muscle of MNUAK1KO mice, as evidenced by increased phosphorylation of IRS1 Tyr-608, AKT Thr-308, and TBC1D4 Thr-649. These observations suggest that a physiological role of NUAK1 is to suppress glucose uptake through negative regulation of insulin signaling in oxidative muscle.

NUAK1 is a serine/threonine kinase belonging to the AMP-activated protein kinase-related kinase (AMPK-RK)[2] family. AMPK is a heterotrimer composed of an α catalytic subunit and two regulatory subunits: β and γ. The AMPK-RK family includes 12 proteins classified together on the basis of sequence similarity with AMPKαs (1, 2). The phosphorylation and activation of AMPKαs are up-regulated by AMP through binding to the γ regulatory subunit (3). On the other hand, AMPK-RKs do not have regulatory subunits; thus their activities are not directly regulated by the cellular AMP:ATP ratio (4). Like the AMPKαs and most other AMPK-RKs, NUAK1 can be phosphorylated by liver kinase B1 (LKB1) at a conserved threonine residue (corresponding to Thr-211 in NUAK1) (2). In addition to Thr-211, NUAK1 can be phosphorylated at Ser-600 by AKT (5). However, a recent study demonstrated that amino acid substitution at this site (S600A) has no influence on kinase activity (6). Thus, the functional significance of phosphorylation at Ser-600 is controversial.

In epithelial cells and fibroblasts, LKB1-NUAK1 phosphorylates myosin phosphatase target subunit 1 and large tumor suppressor homolog 1, which results in cell detachment and senescence, respectively (6, 7). NUAK1 also acts as a transcriptional coactivator in complex with LKB1 and tumor suppressor p53 to induce cell cycle G_1 arrest in A549 lung adenocarcinoma cells (8). In mouse C2C12 myoblasts, NUAK1 is increasingly expressed with differentiation to myotubes (9). Apart from these *in vitro* studies, a study involving knock-out mice showed that the mouse homolog of NUAK1 (OMPHK1) is essential for closure of the ventral body wall in developing embryos (10).

* This work was supported in part by a Grant for the 3rd Term Comprehensive 10-Year Strategy for Cancer Control from the Ministry of Health, Labour and Welfare Japan.
⌘ *Author's Choice*—Final version full access.
[S] This article contains supplemental text, references, mass spectra, and Tables S1–S3.
[1] To whom correspondence should be addressed: Cancer Physiology Project, Research Center for Innovative Oncology, National Cancer Center Hospital East, 6-5-1 Kashiwanoha, Kashiwa, Chiba 277-8577, Japan. Tel.: 81-4-7134-8786; Fax: 81-4-7134-8786; E-mail: hesumi@ncc.go.jp.

[2] The abbreviations used are: AMPK, AMP-activated protein kinase; AMPK-RK, AMPK-related kinase; IRS1, insulin receptor substrate 1; NUAK1, NUAK family SNF1-like kinase 1; TBC1D4, TBC1 domain family member 4; PGC-1α, peroxisome proliferator-activated receptor γ coactivator 1-α; TNNC, troponin C; GLUT4, glucose transporter type 4; GYS1, glycogen synthase 1; TA, tibialis anterior; EDL, extensor digitorum longus; OGTT, oral glucose tolerance test; ITT, insulin tolerance test; NC, normal chow diet; HFD, high fat diet; LKB, liver kinase B1; KHB, Krebs-Henseleit buffer; FDG, fluoro-D-glucose.

In a study with colorectal cancer clinical samples, increased NUAK1 mRNA has been observed (11). Overall, the functions and roles of NUAK1 have been investigated in the context of motility or proliferation of cultured cells, embryonic development, and cancer progression. However, little research has focused on the physiological roles of NUAK1 in adult tissues.

Skeletal muscle is the major tissue responsible for disposal of total body glucose (12). The two major physiological stimulators of skeletal muscle glucose uptake are insulin and muscle contraction (13). Contraction-stimulated glucose uptake has been shown to be mediated by LKB1 via AMPKα2 and/or NUAK2, an AMPK-RK with the highest homology to NUAK1 (14–20). In addition to the influences on contraction-stimulated glucose uptake, muscle-specific LKB1 knock-out mice display increased insulin sensitivity and improved whole body glucose homeostasis (21). In contrast, muscle-specific inhibition of AMPKα2 impairs insulin sensitivity and glucose tolerance (22). Other than AMPKα2 and NUAK2, little is known about the involvement of other AMPK-RKs in muscle glucose metabolism.

The purpose of this study was to elucidate the physiological roles of NUAK1 in adult tissues. For this purpose, we generated muscle-specific NUAK1 knock-out (MNUAK1KO) mice. To our knowledge, this is the first report of conditional knock-out of NUAK1. MNUAK1KO mice were apparently normal but exhibited improved glucose homeostasis under high fat diet (HFD) conditions. To understand the molecular mechanisms underlying the phenotype associated with the knock-out, we performed a quantitative phosphoproteome analysis of skeletal muscle. Our data suggest that one role of NUAK1 is suppression of insulin signal transduction in skeletal muscle.

EXPERIMENTAL PROCEDURES

Animal Protocols—All of the experimental protocols were approved by the Institutional Ethics Review Committee at the National Cancer Center. The mice were maintained on a 12-h light/dark cycle and housed in a temperature-controlled barrier facility with free access to water and a standard rodent chow composed of 20% calories from fat, 50% calories from carbohydrate, and 30% calories from protein (CMF; Oriental Yeast, Tokyo, Japan). *Nuak1*$^{flox/flox}$ mice were obtained from the Laboratory for Animal Resources and Genetic Engineering, Center for Developmental Biology, RIKEN Kobe (accession number CDB0555K). Prior to initiation of the present study, *Nuak1*$^{flox/flox}$ mice were backcrossed onto a C57BL/6J background using the speed cogenic method (Oriental Bioservice, Tokyo, Japan). To generate MNUAK1KO mice, *Nuak1*$^{flox/flox}$ mice were mated with muscle creatin kinase (*Mck*)-*Cre* mice (JAX, number 006475: B6.FVB (129S4)-Tg (Ckmm-cre) 5 Khn/J). As a control for MNUAK1KO mice, their *Nuak1*$^{flox/flox}$ littermate mice were used. For HFD-induced glucose intolerance, the mice were fed a HFD composed of 57% calories from fat, 23% calories from carbohydrate, and 20% calories from protein (HFD32; Clea Japan, Tokyo, Japan) starting from 5 weeks of age until the termination of the experiments. Male mice were used for all of the experiments.

Genotyping—Genomic DNA from various tissues was subjected to PCR involving 34 cycles of denaturation at 94 °C for 30 s, annealing at 60 °C for 30 s, and elongation at 72 °C for 90 s with the following primers: 5′-specific primer P1 (5′-GGTAGGTGGAGGTCGGCTGAGAAGG) and 3′-specific primer P2 (5′-TCGGATCCTAGTGAACCTCTTC).

Real Time RT-PCR—Total RNA was extracted using Isogen (Nippon Gene, Tokyo, Japan) and quantified using a NanoDrop 2000 spectrophotometer (Thermo Fisher Scientific, Waltham, MA). Equal amounts (3.5 μg/15-μl reaction) of total RNA were subjected to first strand cDNA synthesis using a first strand cDNA synthesis kit (GE Healthcare Japan) according to the manufacturer's instructions. Real time PCR was carried out with TaqMan Universal PCR Master Mix (Invitrogen Japan) and TaqMan gene expression assays (Invitrogen Japan) according to the manufacturer's protocols. The TaqMan gene expression assays used in this study were Nuak1 (Mm01250701_m1), Nuak2 (Mm00546961_m1), PGC-1α (Mm_01208835_m1), TNNC1 (Mm00437111_m1), TNNC2 (Mm00437116_m1), and 18 S rRNA (4319413E). For relative quantification, C_t values for each gene were normalized to those for 18 S rRNA. For absolute quantification, synthesized oligonucleotide DNA fragments (Sigma-Aldrich Japan) containing the PCR amplicon regions were used to generate standard curves.

Immunoblotting—Following sacrifice, mouse tissues were rapidly dissected and frozen in liquid nitrogen. The frozen samples were homogenized in lysis buffer containing 1% SDS, 10 mM Tris (pH 7.5), 1 mM Na_3VO_4, and protease inhibitor mixture (Sigma-Aldrich Japan) and then subjected to SDS-PAGE. The proteins were transferred onto a polyvinylidene fluoride microporous membrane (Millipore, MA). The primary antibodies used were: anti-NUAK1 (4458), anti-phospho-LKB1 Ser-428 (3482), anti-LKB1 (3047), anti-IRS1 (2382), anti-phospho-AKT Thr-308 (9275), and anti-AKT (4685), all obtained from Cell Signaling Technologies (Beverly, MA), anti-phospho-TBC1D4 Thr-642 (ab65753), and anti-glucose transporter type 4 (GLUT4) (ab65976), obtained from Abcam (Cambridge, UK), anti-TBC1D4 (07-741) and anti-phospho-IRS1 Tyr-608 (09-432), obtained from Millipore (Billerica, MA), and anti-actin (sc-1615), obtained from Santa Cruz Biotechnology (Santa Cruz, CA). Immunoblots were scanned using a Canoscan LiDE60 image scanner (Cannon, Tokyo, Japan), and the intensities of the protein bands were quantified using an image processing program ImageJ 1.44.

Measurements of Blood Glucose, Insulin, and Muscle Glycogen—Blood glucose levels were measured from tail blood using an Antsense II glucometer (Bayer Medical, Tokyo, Japan). Plasma insulin levels were determined from peripheral blood using mouse insulin ELISA kit S-Type (Shibayagi, Gunma, Japan). The glycogen concentration of the soleus muscle was determined using a glycogen assay kit (BioVision, Milpitas, CA). For oral glucose tolerance tests (OGTT), mice fasted overnight were administered glucose at a dose of 1 g/kg of body weight. Blood glucose levels were measured immediately before and 20, 40, 60, and 120 min after the administration. For insulin tolerance tests (ITT), mice fasted for 2 h were injected intraperitoneally with recombinant human insulin (Wako Pure Chemical Industries, Osaka, Japan) at a dose of 1 unit/kg of

body weight. Blood glucose levels were measured immediately before and 15, 30, and 60 min after the injection.

Histological Analysis—Soleus muscles were fixed with 10% neutral buffered formalin, embedded in paraffin, and sectioned at 6-μm thickness. The sections were stained using Alexa Fluor 555-conjugated wheat germ agglutinin and Hoechst 33342 (Invitrogen Japan). The immunofluorescent images were visualized with a Zeiss LSM 710 confocal laser microscope (Carl Zeiss Japan). The myocyte cross-sectional areas obtained from 84 cells from six control mice and 83 cells from six MNUAK1KO mice were quantified by ZEN 2009 image viewer software (Carl Zeiss Japan).

Measurements of Glucose Uptake in Skeletal Muscles—All of the incubation media were pregassed with 95% O_2, 5% CO_2, and all incubation was performed at 30 °C. *Ex vivo* muscle incubation was performed as described previously (23). Soleus muscles were incubated for 30 min in Krebs-Henseleit buffer (KHB) (pH 7.4) containing 10 mM HEPES, 5.5 mM glucose, 2 mM pyruvate, and 0.05% free fatty acid free-bovine serum albumin without or with insulin (20 milliunits/ml). Subsequently, the muscles were washed with glucose-free KHB without or with insulin (20 milliunits/ml) three times. Glucose transport was then determined in KHB supplemented with 0.5 MBq/ml 2-deoxy-2-[^{18}F]fluoro-D-glucose ([^{18}F]FDG) (Nihon Medi-Physics, Tokyo, Japan), 0.75 mM FDG, and 9 μM mannitol in the absence or presence of insulin (20 milliunits/ml) for 20 min. [^{18}F]FDG was washed out with ice-cold KHB without glucose and without insulin three times. Thereafter, the muscles were blotted and weighed. The remaining radioactivity derived from [^{18}F]FDG was measured by a Wizard 2 automatic γ-counter (PerkinElmer Japan).

Phosphoproteome Analysis—Soleus muscles were frozen in liquid nitrogen and disrupted using a multibead shocker (MB400U; Yasui Kikai, Osaka, Japan). Homogenates of the muscles were reduced with dithiothreitol and then alkylated with iodoacetamide before being subjected to a dual enzymatic digestion (Lys-C followed by trypsin) (24). Digested samples were desalted using StageTips with SDB-XC Empore disk membranes (3M Company, St. Paul, MN) (25). Dimethyl labeling was performed according to the literature (26). Phosphopeptide enrichment based on hydroxy acid-modified metal oxide chromatography was performed using lactic acid-modified titania as described previously with a slight modification (27). The eluates from hydroxy acid-modified metal oxide chromatography were concentrated in a vacuum evaporator (CC-105; Tomy, Tokyo, Japan). NanoLC-MS/MS analysis was performed using a previously described setup (28). Peptides and proteins were identified by Mascot version 2.3 (Matrix Science, Tokyo, Japan) against the Uniprot/SwissProt data base release 2011_04 with a precursor mass tolerance of 3 ppm, a fragment ion mass tolerance of 0.8 Da, and strict trypsin specificity allowing for up to two missed cleavages. Cysteine carbamidomethylation was set as a fixed modification. Oxidation of methionine, phosphorylation of serine, threonine, and tyrosine, and [$^1H_4$,$^{12}C_2$/$^2H_4$,$^{13}C_2$]dimethylation of the N terminus and lysine were allowed as variable modifications. Peptides were considered identified if the Mascot score was over the 95% confidence limit based on the "identity" score of each peptide, and at least three successive y or b ions and two or more y, b, and/or precursor origin neutral loss ions were observed, based on the error-tolerant peptide sequence tag concept (29). False positive rates were estimated by searching against a randomized decoy data base created by the Mascot Perl program supplied by Matrix Science (averaged false positive rate = 1.02%). The details of experimental procedures are described in the supplemental information.

RESULTS

NUAK1 Is Preferentially Expressed in Highly Oxidative Tissues Such as Cerebrum, Heart, and Soleus Muscle—To determine the tissue distribution of NUAK1, the level of mouse Nuak1 mRNA in various organs and tissues was measured using quantitative RT-PCR. The distribution of Nuak2 mRNA was also examined because NUAK1 and NUAK2 may have redundant functions (7, 30). As shown in Fig. 1*A*, Nuak1 was most abundant in the cerebrum and heart, which is consistent with the distribution of human NUAK1 (31). We found that among the skeletal muscles examined, Nuak1 was selectively expressed in the soleus, at a level comparable with the heart. In contrast, Nuak2 was barely detectable in the skeletal muscles and was highly expressed in kidney.

Expression of NUAK1 protein in the heart, soleus, tibialis anterior (TA), and extensor digitorum longus (EDL) muscles was analyzed using immunoblotting, which also showed muscle type-specific expression of NUAK1 (Fig. 1*B*). LKB1 was expressed in all of the muscles examined, and the phosphorylation level was lower in the heart than in the other muscles (Fig. 1*B*). Previous studies have shown that soleus muscle predominantly contains type I and type IIA fibers, which have a high mitochondrial density and oxidative capacity (32). Therefore, our data suggest that NUAK1 is preferentially expressed in highly oxidative tissues such as the cerebrum, heart, and soleus muscle.

Generation of MNUAK1KO Mice—To investigate the role of NUAK1 in skeletal muscle, we generated conditional knockout (MNUAK1KO) mice. Mice carrying Nuak1 floxed allele (*Nuak1$^{flox/flox}$*), in which exon 3 was flanked by *loxP* sequences as shown in Fig. 1*C*, were crossed with muscle creatin kinase (*Mck*)-*Cre* transgenic mice. The MNUAK1KO mice were born in a normal Mendelian ratio and had no gross abnormalities in appearance and behavior. Genomic PCR analysis confirmed deletion of the Nuak1 gene in the heart and skeletal muscles of MNUAK1KO mice. The deletion was not observed in any non-muscle tissues in the MNUAK1KO mice or in tissues from their *Nuak1$^{flox/flox}$* (control) littermates (Fig. 1*D*). Real time RT-PCR showed that the level of Nuak1 mRNA was substantially reduced in heart, soleus, TA, and EDL muscles of MNUAK1KO mice (Fig. 1*E*). The NUAK1 protein was barely detectable in those tissues of MNUAK1KO mice (Fig. 1*F*). These observations confirmed that muscle-specific knock-out of NUAK1 was achieved.

MNUAK1KO Mice Exhibit No Skeletal Muscle Morphological Abnormalities—For phenotypic analysis, we first assessed the mass and fiber size of the soleus muscle, as well as the weight of heart and body, because the involvement of NUAK1 in myoblast differentiation has been implied (9). No difference was

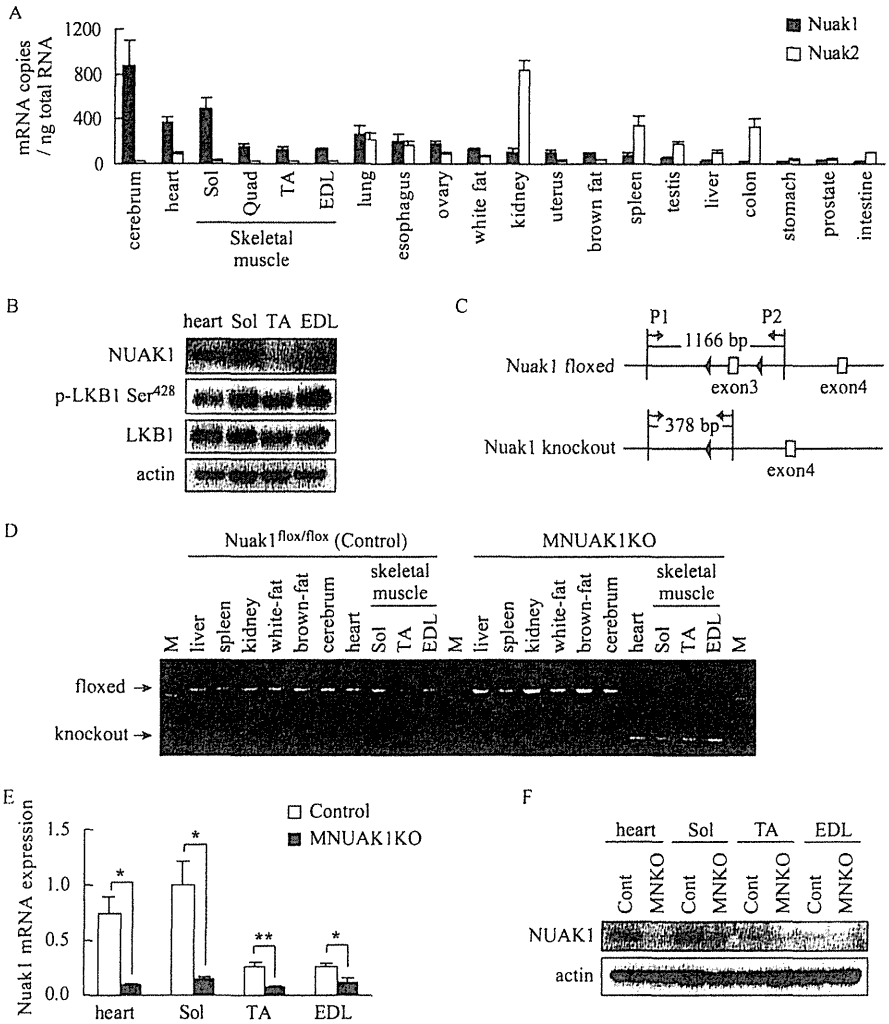

FIGURE 1. **NUAK1 is preferentially expressed in highly oxidative tissues.** *A*, quantitative RT-PCR analysis of Nuak1 and Nuak2. RNA was isolated from 10-week-old C57BL/6 mice. The data are the means ± S.E. ($n = 3$). *B*, immunoblotting analysis of NUAK1 and LKB1 in heart, Sol, TA, and EDL muscles. Actin was used as a loading control. Protein extracts were from three individual 10-week-old C57BL/6 mice. *C*, schematic representation of floxed and knock-out alleles of Nuak1. The *black arrowheads* represent *loxP* sites. *Gray arrows* indicate PCR primers P1 and P2 used for the genotyping. Amplification with the P1 and P2 primers yields the 1166-bp product from the floxed allele and the 378-bp product from the knock-out allele. *D*, genotyping of Nuak1 floxed mice without (control) or with (MNUAK1KO) the *Mck-Cre* transgene. *M*, molecular marker. *E*, real time RT-PCR for Nuak1 mRNA in muscles. RNA was isolated from 10-week-old control and MNUAK1KO mice. The mRNA levels are expressed relative to that in soleus muscle of control mice. The data are the means ± S.E. ($n = 3$). *, $p < 0.05$; **, $p < 0.01$ (Student's *t* test). *F*, immunoblot analysis of NUAK1 protein in muscles. Protein extracts of each type of muscle were prepared from three individual mice. *Sol*, soleus; *Quad*, quadriceps; *Cont*, control; *MNKO*, MNUAK1KO.

observed between MNUAK1KO and control mice with respect to body, heart, or soleus weights under both normal chow diet (NC) and HFD conditions at 13–15 weeks of age (Fig. 2, *A* and *B*, and supplemental Table S1). The myocyte cross-sectional area of the soleus muscle was almost identical in MNUAK1KO and control mice (Fig. 2*C*). The expression of NUAK1 in heart or soleus muscle of control mice was not affected by the HFD (data not shown).

To determine whether NUAK1 is involved in the formation of type I fibers, we examined the expression level of peroxisome proliferator-activated receptor γ coactivator 1-α (PGC-1α), a transcriptional regulator that drives type I fiber formation (33). We also assessed myofiber composition by examining the expression levels of troponin C1 (TNNC1) and troponin C2 (TNNC2), which are specifically expressed in type I and type II fibers, respectively (32). Real time RT-PCR analysis revealed no significant difference between MNUAK1KO and control mice with respect to PGC-1α, TNNC1, or TNNC2 mRNA expression in the soleus, TA, and EDL muscles (Fig. 2, *D–F*). These observations suggest that NUAK1 is not involved in the determination of muscle mass, fiber size, or fiber type.

MNUAK1KO Mice Fed High Fat Diet Exhibit Improved Glucose Homeostasis—To assess the influence of muscle-specific knock-out of NUAK1 on whole body glucose homeostasis, MNUAK1KO and control mice were fed either a NC or a HFD, and the level of blood glucose was monitored. There was no difference in the fasting blood glucose concentration of MNUAK1KO and control mice fed a NC through age 19 weeks (Fig. 3, *A* and *B*). In contrast, on a HFD, the fasting blood glucose concentration at 13–15 weeks of age was significantly lower in MNUAK1KO mice than in control mice (Fig. 3*A*). This phenotype was even more prominent by age 18–19 weeks (Fig. 3*B*). At this age, MNUAK1KO mice fed a HFD exhibited slightly lower body weight compared with that of control mice

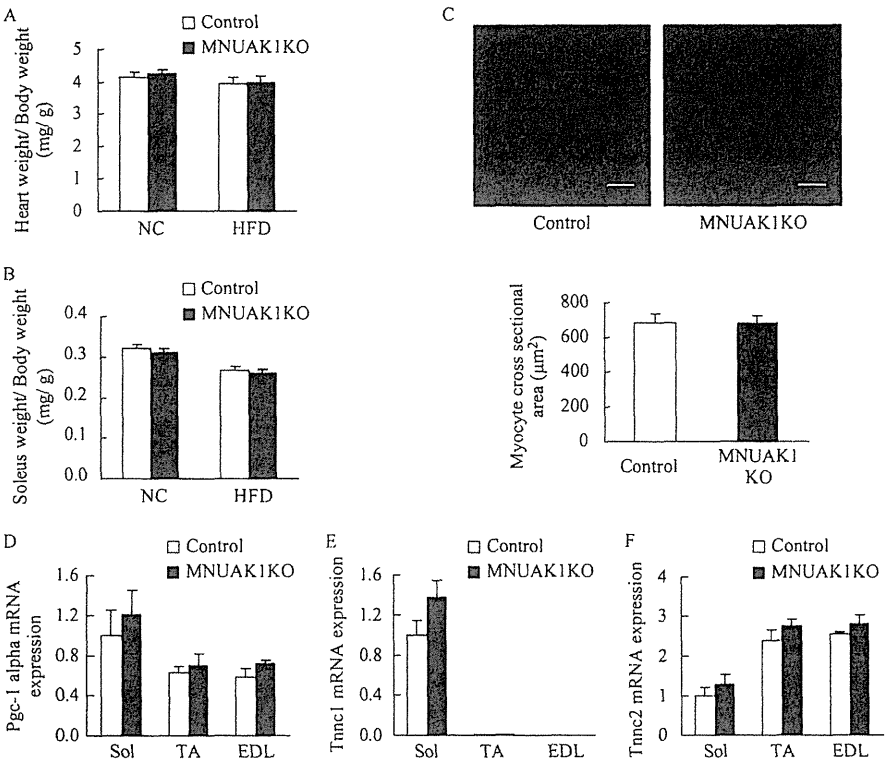

FIGURE 2. **MNUAK1KO mice display no morphological abnormalities.** *A* and *B*, weight of heart (*A*) and soleus muscle (*B*) of control and MNUAK1KO mice fed a NC or HFD. The indicated values are normalized to body weight. The data are the means ± S.E. (n = 10). *C*, cross-section of soleus muscle myocytes stained with wheat germ agglutinin. *Scale bars*, 20 μm. The graph below shows the average myocyte cross-sectional area for control and MNUAK1KO mice. The data are the means ± S.E. (n = 6). *D–F*, real time RT-PCR analysis of PGC-1α (*D*), TNNC1 (*E*), and TNNC2 (*F*). The mRNA levels are expressed relative to that of the soleus in control mice. The data are the means ± S.E. (n = 3). Mice at the age of 13–15 weeks were used for all experiments. *Sol*, soleus.

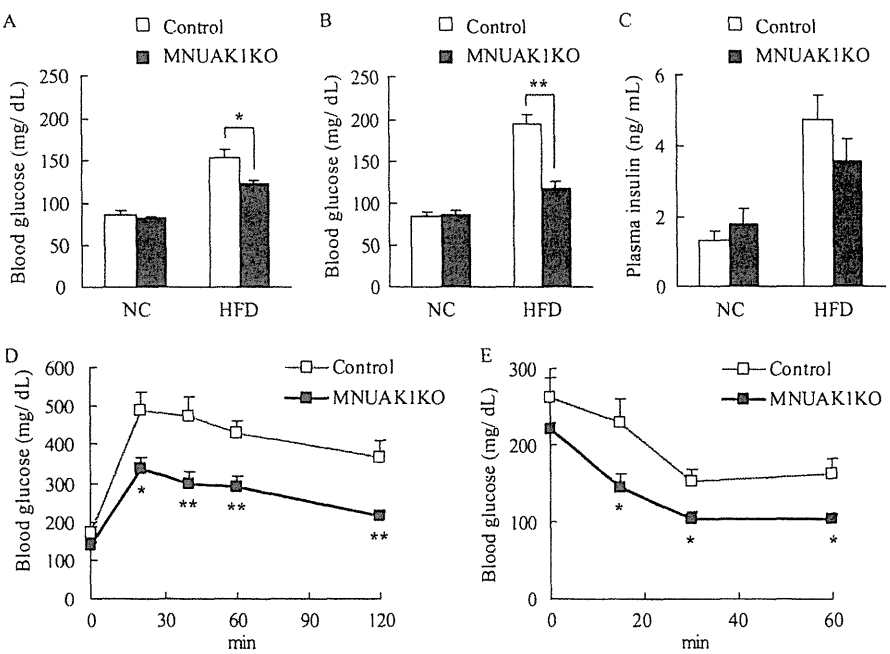

FIGURE 3. **MNUAK1KO mice show improved glucose homeostasis under HFD conditions.** *A* and *B*, fasting blood glucose levels of control and MNUAK1KO mice at 13–15 weeks (*A*) and 18–19 weeks of age (*B*). The data are the means ± S.E. (n = 8). *C*, plasma insulin levels of control and MNUAK1KO mice. The data are the means ± S.E. (n = 12). *D*, oral glucose tolerance of control and MNUAK1KO mice under HFD conditions. The data are the means ± S.E. (n = 12). *E*, insulin tolerance of control and NUAK1 KO mice under HFD conditions. The data are the means ± S.E. (n = 8). Mice at the age of 13–15 weeks were used for *C–E*. *, $p < 0.05$; **, $p < 0.01$ (Student's t test).

(supplemental Table S1), which may reflect the improved glucose homeostasis in MNUAK1KO mice. In conjunction with these findings, the fasting plasma free fatty acid level was significantly lower in MNUAK1KO mice than in control mice under HFD conditions (supplemental Table S1). The HFD-induced hyperinsulinemia and hypertriglyceridemia also tended

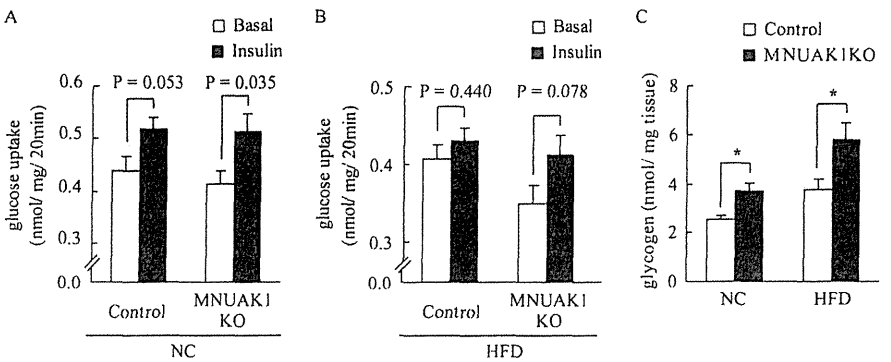

FIGURE 4. **MNUAK1KO mice show improved insulin sensitivity and increased glycogen storage in skeletal muscle.** *A* and *B*, rate of glucose uptake in soleus muscles isolated from 18–20-week-old control and MNUAK1KO mice fed a NC (*A*) or a HFD (*B*) without or with insulin stimulation. The data are the means ± S.E. ($n = 7$ for NC and 8 for HFD). *C*, glycogen concentration in the soleus muscle of 13–15-week-old control and MNUAK1KO mice fed a NC or HFD. The data are the means ± S.E. ($n = 8$). *, $p < 0.05$ (Student's *t* test).

to be less pronounced in MNUAK1KO mice (Fig. 3*C* and supplemental Table S1). The level of food intake was unaltered between MNUAK1KO and control mice (supplemental Table S1).

To further investigate the involvement of NUAK1 in glucose homeostasis, an oral glucose tolerance test (OGTT) and an insulin tolerance test (ITT) were performed. No differences in OGTT and ITT results were observed between MNUAK1KO and control mice fed a NC (data not shown). On a HFD, MNUAK1KO mice displayed significantly lower blood glucose levels than control mice as determined using both the OGTT (Fig. 3*D*) and the ITT (Fig. 3*E*). These results indicate that muscle-specific knock-out of NUAK1 increases the capacity for glucose disposal, at least in part, in response to insulin.

To determine whether the improved whole body glucose metabolism is attributed to NUAK1-deficient skeletal muscle, we measured glucose uptake into isolated soleus muscle without or with insulin. Insulin-stimulated glucose uptake was observed in the soleus muscle from both MNUAK1 and control mice fed a NC (Fig. 4*A*). Under HFD conditions, the effects of insulin were less pronounced in the soleus muscle from control mice, whereas NUAK1-deficient soleus muscle displayed insulin-stimulated glucose uptake comparable with that observed under NC conditions (Fig. 4*B*). We also measured the soleus muscle glycogen concentration in MNUAK1KO and control mice. The glycogen concentration was significantly higher in the soleus of MNUAK1KO mice under both NC and HFD conditions, indicating that NUAK1 plays a critical role in glucose storage in the soleus muscle (Fig. 4*C*). Taken together, our findings suggest that a muscle-specific knock-out of NUAK1 preserved insulin sensitivity under HFD conditions.

Phosphorylation of TBC1D4 Is Increased by Deletion of Nuak1 in Skeletal Muscle—Glucose metabolism in skeletal muscle is highly sensitive to both the expression of glucose transporter type 4 (GLUT4) which is increased by exercise and decreased by a HFD (34, 35), and its translocation to the plasma membrane (36–38), which is facilitated by phosphorylated TBC1 domain family member 4 (TBC1D4) (39, 40). To investigate the molecular mechanism underlying improved glucose metabolism, the TBC1D4 phosphorylation in acute response to glucose in the soleus of HFD-fed MNUAK1KO and control mice was examined. The level of GLUT4 protein was also

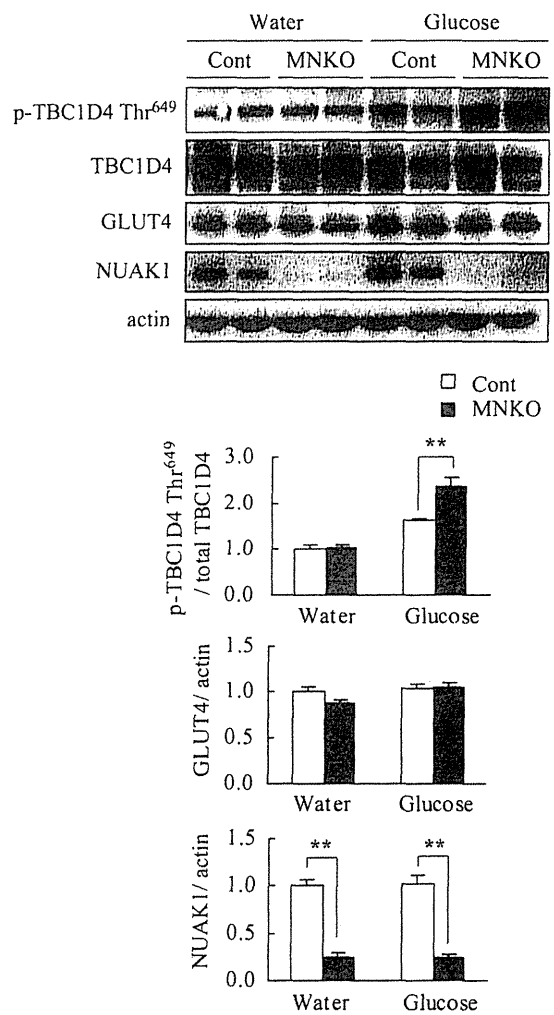

FIGURE 5. **Phosphorylation of TBC1D4 is up-regulated in NUAK1-deficient muscle after glucose administration.** Immunoblot analysis of TBC1D4, GLUT4, and NUAK1 in soleus muscle of HFD-fed control and MNUAK1KO mice. Mice at the age of 13–15 weeks were fasted overnight and sacrificed 40 min after oral administration of water (basal control) or glucose. The graphs show the intensities of phospho-TBC1D4, GLUT4, and NUAK1 bands. Phospho-TBC1D4 protein levels were normalized to total TBC1D4. GLUT4 and NUAK1 protein levels were normalized to actin. The protein levels are expressed relative to those in the water-administered control mice. The data are the means ± S.E. ($n = 4$ for NUAK1 and 5 for TBC1D4 and GLUT4). **, $p < 0.01$ (Student's *t* test). *Cont*, control; *MNKO*, MNUAK1KO.

TABLE 1

Phosphoproteome analysis in soleus muscles from MNUAK1KO and control mice fed a HFD

The listed phosphorylation sites were differentially regulated more than 2.0-fold in MNUAK1KO mice compared with control mice under HFD conditions. The data are means ± S.E. (n = 4).

Symbol	Name	Potential phosphorylation-sites in unique peptides	KO/Control ratio
Phosphoproteins decreased in MNUAK1KO			
Glucose metabolism			
PKCtheta	Protein kinase C theta type	S676[b]	**0.40** ± 0.13
IRS1	Insulin receptor substrate 1	S1097[b]	**0.10** ± 0.03
GYS1	Glycogen [starch] synthase, muscle	S652, S657[b]	**0.42** ± 0.04
		S653[b], S657[b]	**0.50** ± 0.05
Actin-myosin cytoskeleton			
MYH1/ 4/ 6/ 7/ 8[a]	Myosin-1/ 4/ 6/ 7/ 8	S1044/ S1041/ S1039/ S1037/ S1040	**0.33** ± 0.09
TTN	Titin	S322	**0.47** ± 0.07
		S2078, S2080	**0.48** ± 0.07
TCAP	Telethonin	S39	**0.47** ± 0.07
CTNNA1	Catenin alpha-1	S641[b]	**0.30** ± 0.09
SYNPO2L	Synaptopodin 2-like protein	T138, S140	**0.40** ± 0.07
CMYA5	Cardiomyopathy-associated protein 5	S769	**0.37** ± 0.06
PLEC	Plectin	S4629, Y4618 or Y4619 or S4620[c]	**0.27** ± 0.03
		S4392, S4393, S4396	**0.34** ± 0.04
		S4620, S4633	**0.37** ± 0.08
		Y4622, S4629	**0.37** ± 0.08
		Y4622, S4627	**0.42** ± 0.05
		Y4619, S4627	**0.42** ± 0.06
		Y4622, T4630	**0.44** ± 0.01
		S4392, S4393	**0.48** ± 0.05
		Y4622, S4625	**0.49** ± 0.03
Protein biosynthesis			
EIF5B	Eukaryotic translation initiation factor 5B	S108, S114	**0.34** ± 0.07
RPLP2	60S acidic ribosomal protein P2	S105[b]	**0.34** ± 0.03
DNAJC1	DnaJ homolog subfamily C member 1	S477, S478	**0.41** ± 0.04
Miscellaneous			
LNP	Protein lunapark	S411	**0.35** ± 0.05
STEAP3	Metalloreductase STEAP3	S17, S20	**0.33** ± 0.04
GOGA4	Golgin subfamily A member 4	T39, S41	**0.41** 0.03
UBP2L	Ubiquitin-associated protein 2-like	S497, S480 or T481 or S482[c]	**0.31** ± 0.03
Phosphoproteins increased in MNUAK1KO			
Actin-myosin cytoskeleton			
LRRC39	Leucine-rich repeat-containing protein 39	S328	**2.20** ± 0.07
ANKRD2	Ankyrin repeat domain-containing protein 2	S347, T351	**3.63** ± 0.69
Protein biosynthesis			
EIF5B	Eukaryotic translation initiation factor 5B	S137	**4.23** 1.27
Miscellaneous			
HMGA1	High mobility group protein HMG-I/HMG-Y	S102, S103	**2.22** ± 0.46
PACSIN3	Protein kinase C and casein kinase II substrate protein 3	S354	**2.32** ± 0.32
2310046A06RIK	Uncharacterized protein C6orf142 homolog	S85	**2.01** ± 0.25

[a] Protein isoforms that could not be distinguished by unique peptides.
[b] Phosphorylation sites previously identified using site-specific methods in reference to the PhosphoSitePlus database.
[c] Ambiguous phosphorylation sites (*i.e.*, those that could not be determined from MS-MS spectra).

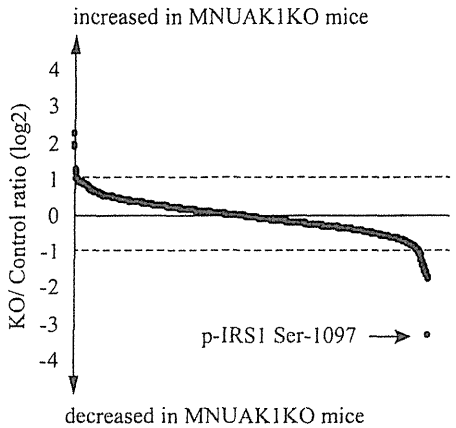

FIGURE 6. **Phosphoproteome of soleus muscles from MNUAK1KO and control mice.** A total of 1,229 phosphopeptides were quantitatively detected in soleus muscle. KO/control ratio of phosphopeptides are shown by *blue dots* (mean, $n = 4$). Phosphopeptides with KO/control ratio of more than 2.0 or less than 0.5 are listed in Table 1. An IRS1 phosphopeptide containing Ser-1097 is indicated by an *arrow*.

compared between MNUAK1KO and control mice. The phosphorylation level of TBC1D4 Thr-649 (corresponding to Thr-642 in the human isoform) was significantly higher in the soleus muscle from MNUAK1KO mice in the glucose-administered group (Fig. 5). This difference was not observed in the water-administered group, suggesting that postprandial glucose uptake is enhanced in the soleus of MNUAK1KO mice. No differences were observed in the GLUT4 protein level (Fig. 5). Our data indicate that the observed increase in glucose disposal in MNUAK1KO mice fed a HFD is associated with increased GLUT4 translocation rather than changes in GLUT4 expression in the soleus muscle.

Insulin Signal Transduction Is Enhanced in Soleus Muscle of MNUAK1KO Mice—To obtain a comprehensive understanding of the molecular mechanism underlying the observed MNUAK1KO phenotype, a quantitative phosphoproteome analysis was performed on soleus muscle isolated from HFD-fed MNUAK1KO and control mice in random fed state. Total protein was enzymatically digested, differentially labeled with stable isotopes, and then subjected to simultaneous LC-MS/MS analysis, which allowed for precise comparison between the two samples. To ensure reproducibility, four independent experiments were performed. All of the mass spectra and a detailed list of all proteins identified in this study are provided in the supplemental mass spectra and supplemental Table 3, respectively. Table 1 shows proteins that were found to be differentially phosphorylated more than 1.5-fold in all four experiments and more than 2-fold in average between MNUAK1KO and control mice. Among the 1,229 phosphopeptides quantitatively detected, the abundance of 27 phosphopeptides, corresponding to 21 proteins, decreased as a result of the Nuak1 deletion, whereas the abundance of six phosphopeptides, corresponding to six proteins, increased. Most of the differences in phosphorylation status were also observed under NC conditions (supplemental Table S2). It should be noted that differential regulation of phosphoproteins involved in glucose metabolism was clearly shown. In particular, the phosphorylation of IRS1 at Ser-1097 was changed most drastically (KO/control ratio = 0.10 ± 0.03) (Fig. 6). This serine phosphorylation (Ser-1101 in the human isoform), together with the phosphorylation of its upstream regulator PKCθ at Ser-676 (the same residue in the human isoform), is known to mediate negative feedback regulation of insulin signaling through blocking of IRS1 tyrosine phosphorylation (41). Phosphorylation of glycogen synthase 1 (GYS1) at the C-terminal serine residues including Ser-653 and Ser-657 (both same in the human isoform) leads to its inactivation and decreases glycogen synthesis (42, 43). Therefore, the hypophosphorylation of these sites in NUAK1-deficient soleus muscle can enhance insulin sensitivity and glycogen synthesis, which is consistent with the observed decreased blood glucose, improved glucose tolerance and insulin sensitivity, and increased muscle glycogen content phenotype. Besides glucose metabolism, biological processes shown to be affected include cell motility. Components of the actin-myosin cytoskeleton, such as various myosin isoforms, titin, and plectin, were also hypophosphorylated in NUAK1-deficient soleus muscle. Although it is unclear how changes in the phosphorylation status of these cytoskeletal proteins affect glucose metabolism and muscle contraction, the data suggest that NUAK1 has a role in regulation of muscle cytoskeletal structure.

To validate the increased insulin signaling suggested by the phosphoproteome analysis, phosphorylation of IRS1 at Tyr-608 and AKT at Thr-308 in soleus muscle of mice fed a HFD were analyzed by immunoblotting. The phosphorylation levels of IRS1 and AKT were significantly higher in soleus muscle of MNUAK1KO mice than in that of control mice under fed conditions, confirming the enhancement of insulin signaling by a lack of NUAK1 (Fig. 7*A*). We also examined the phosphorylation of IRS1 and AKT in acute response to glucose and insulin in soleus muscle of mice fed a HFD. As shown in Fig. 7*B*, phosphorylation levels of IRS1 Tyr-608 and AKT Thr-308 in response to glucose administration were significantly higher in soleus muscle of MNUAK1KO mice than in that of control mice. The AKT Thr-308 phosphorylation in response to insulin injection was also significantly higher in the soleus muscle of MNUAK1KO mice than in that of control mice (Fig. 7*C*). No difference was observed in IRS1 phosphorylation in response to insulin injection, probably because of the time point for this analysis. Note that phosphorylation level of AKT under basal (fasted) conditions was significantly lower in soleus muscle of MNUAK1KO mice than in that of control mice (Fig. 7, *B* and *C*). An increase in the basal phosphorylation level of AKT is characteristic of insulin resistance induced by a HFD (44, 45). These observations strongly suggest that a HFD-induced insulin resistance was reduced in soleus muscle of MNUAK1KO mice. Therefore, we concluded that NUAK1 is involved in the negative regulation of insulin signal transduction in soleus muscle.

DISCUSSION

Skeletal muscle is the principle tissue for insulin-mediated glucose uptake. Oxidative muscle has higher insulin-stimulated glucose transport activity than does glycolytic muscle (46). Therefore, our finding that NUAK1 is highly expressed in soleus muscle as well as cerebrum and heart, which are also highly oxidative tissues, suggests the possibility that NUAK1 is involved in energy metabolism in oxidative tis-

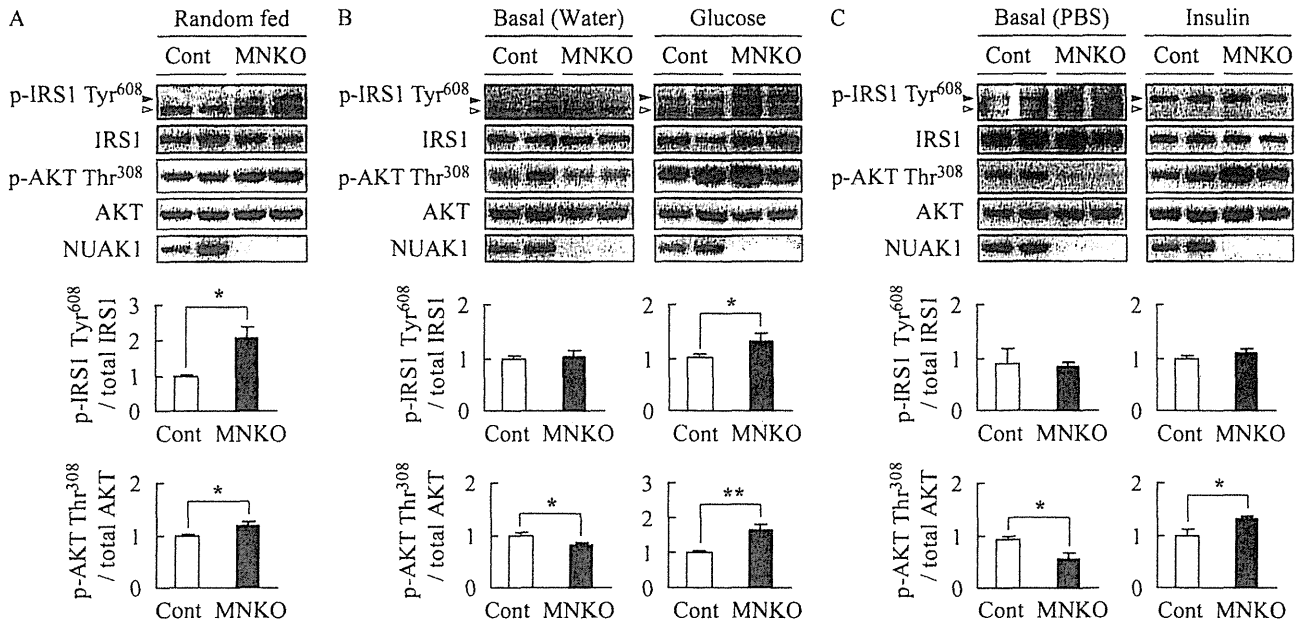

FIGURE 7. **Phosphorylation of insulin signaling proteins are up-regulated in NUAK1-deficient muscle.** Immunoblot analysis of phosphorylation of IRS1 at Tyr-608 (*black arrowhead*) and AKT at Thr-308 in soleus muscle of HFD-fed control and MNUAK1KO mice. A *white arrowhead* denotes a nonspecific band. Graphs show the intensities of phospho-protein bands normalized to total protein levels in each case. The data are expressed relative to those from control mice. *, $p < 0.05$; **, $p < 0.01$ (Student's *t* test). *A*, mice under fed conditions. The data are the means ± S.E. ($n = 3$). *B*, mice were fasted overnight and administered water or glucose (1 g/kg of body weight). Soleus was excised 40 min after the administration. The data are the means ± S.E. ($n = 6$). *C*, mice were fasted overnight and intraperitoneally injected with PBS or insulin (1.5 units/kg of body weight). Soleus was excised 20 min after the injection. The data are the means ± S.E. ($n = 3$). *Cont*, control; *MNKO*, MNUAK1KO.

sues. In support of this hypothesis, muscle-specific LKB1 knock-out (MLKB1KO) mice show improved whole body glucose homeostasis (21). Thus, we examined whether muscle-specific deletion of Nuak1 affects whole body glucose homeostasis and found that MNUAK1KO mice fed a HFD exhibit decreased fasting blood glucose levels and improved glucose metabolism compared with control mice also fed a HFD. The phenotypic similarity, together with the results of previous *in vitro* studies (2, 6, 7), strongly suggests that LKB1 is an upstream kinase of NUAK1 in skeletal muscle. Note that the phenotype of MNUAK1KO mice was apparent only under HFD conditions. This can be explained by the contribution of skeletal muscle to whole body glucose disposal. Under euglycemic conditions, the majority of glucose disposal occurs in a non-insulin-mediated manner, and skeletal muscle accounts for only 20% of whole body glucose disposal (47, 48). On the other hand, skeletal muscle is responsible for virtually all glucose disposal increased in hyperglycemic conditions (47). We concluded that a lack of NUAK1 alters muscle glucose metabolism, which contributes significantly to whole body glucose disposal in mice with hyperglycemia.

Our data provide evidence suggesting that NUAK1 controls glucose metabolism through negative regulation of insulin signal transduction in skeletal muscle. Firstly, the lower blood glucose of MNUAK1KO mice in OGTT and ITT indicates increased insulin sensitivity. Secondly, the *ex vivo* experiment of muscle glucose uptake suggests that NUAK1-deficient muscle is protected from HFD-induced insulin resistance. Thirdly, decreased phosphorylation of PKCθ at Ser-676 and IRS1 at Ser-1097 in the soleus muscle of MNUAK1KO mice indicates that a negative feedback regulation of insulin signal transduction is down-regulated by a lack of NUAK1. Indeed, phosphorylation of IRS1 at Tyr-608, which is caused by insulin and leads to the activation of downstream molecules such as AKT and TBC1D4, was up-regulated in the soleus muscle of MNUAK1KO mice. Our observations in MNUAK1KO mice are consistent with a report that PKCθ knock-out mice are not susceptible to HFD-induced insulin resistance (49). The hypophosphorylation of PKCθ in NUAK1-deficient soleus muscle also explains our observation that basal glucose uptake in muscle tended to be decreased by a lack of NUAK1 (Fig. 4, *A* and *B*), because it is regulated by PKC isoforms (50, 51). Lastly, increased muscle glycogen concentration together with decreased phosphorylation of GYS1 at Ser-653 and Ser-657, which is involved in activation of GYS1, can be explained by enhancement of insulin signaling because GYS1 at Ser-653 is regulated by glycogen synthase kinase 3, a downstream effector of IRS1-AKT axis (42).

How does NUAK1 control the negative feedback loop of insulin signaling? Phosphoproteome analysis showed that phosphorylation of IRS1 at Ser-1097 was decreased remarkably among all phosphorylations in soleus muscle. In adipose tissues, IRS1 is regulated by salt-inducible kinase 2, another member of the AMPK-RK family (52), through phosphorylation of Ser-794. Therefore, although the amino acid sequence flanking Ser-1097 is not consistent with the optimal motif for phosphorylation by AMPK (53–55), it is plausible that IRS1 is a target of NUAK1. The hypophosphorylation of PKCθ, an upstream kinase of IRS1 Ser-1097, can be explained by the lower plasma free fatty acid levels in MNUAK1KO mice because the phosphorylation of PKCθ is stimulated by free fatty acid (56–58).

Our phosphoproteome analysis also revealed that deletion of Nuak1 leads to a decrease in phosphorylation of components of contraction apparatus such as myosin isoforms and titin, which is consistent with a recent report suggesting that myosin and

paramyosin are potential substrates of UNC-82, a *Caenorhabditis elegans* ortholog of NUAK1 and NUAK2 (59). Current understanding of how changes in the phosphorylation status of cytoskeletal proteins affect glucose metabolism and muscle contraction is incomplete. Further phenotypic analyses of cytoskeletal organization and muscle contraction are required to fully understand the role of NUAK1 in skeletal muscle.

In summary, we found that NUAK1 is preferentially expressed in highly oxidative tissues such as the cerebrum, heart, and soleus muscle. We generated muscle-specific NUAK1 knock-out mice and found that they have improved glucose homeostasis compared with control mice when fed a hyperglycemia-inducing HFD. This phenotype is similar to that of muscle-specific LKB1 knock-out mice, suggesting that LKB1 is an upstream kinase for NUAK1 in skeletal muscle. A quantitative phosphoproteome analysis revealed that NUAK1 is involved in the negative feedback regulation of insulin signal transduction, possibly through the phosphorylation of IRS1. Our results strongly suggest that a physiological role of NUAK1 is to suppress insulin-mediated glucose uptake in skeletal muscle.

Acknowledgments—We thank Dr. Izumi O. Umeda and Dr. Hirofumi Fujii (Functional Imaging Division, Research Center for Innovative Oncology, National Cancer Center Hospital East, Kashiwa, Japan) for invaluable advice for the ex vivo glucose uptake experiment.

REFERENCES

1. Manning, G., Whyte, D. B., Martinez, R., Hunter, T., and Sudarsanam, S. (2002) The protein kinase complement of the human genome. *Science* **298,** 1912–1934
2. Lizcano, J. M., Göransson, O., Toth, R., Deak, M., Morrice, N. A., Boudeau, J., Hawley, S. A., Udd, L., Mäkelä, T. P., Hardie, D. G., and Alessi, D. R. (2004) LKB1 is a master kinase that activates 13 kinases of the AMPK subfamily, including MARK/PAR-1. *EMBO J.* **23,** 833–843
3. Scott, J. W., Ross, F. A., Liu, J. K., and Hardie, D. G. (2007) Regulation of AMP-activated protein kinase by a pseudosubstrate sequence on the γ subunit. *EMBO J.* **26,** 806–815
4. Al-Hakim, A. K., Göransson, O., Deak, M., Toth, R., Campbell, D. G., Morrice, N. A., Prescott, A. R., and Alessi, D. R. (2005) 14-3-3 cooperates with LKB1 to regulate the activity and localization of QSK and SIK. *J. Cell Sci.* **118,** 5661–5673
5. Suzuki, A., Kusakai, G., Kishimoto, A., Lu, J., Ogura, T., Lavin, M. F., and Esumi, H. (2003) Identification of a novel protein kinase mediating Akt survival signaling to the ATM protein. *J. Biol. Chem.* **278,** 48–53
6. Humbert, N., Navaratnam, N., Augert, A., Da Costa, M., Martien, S., Wang, J., Martinez, D., Abbadie, C., Carling, D., de Launoit, Y., Gil, J., and Bernard, D. (2010) Regulation of ploidy and senescence by the AMPK-related kinase NUAK1. *EMBO J.* **29,** 376–386
7. Zagórska, A., Deak, M., Campbell, D. G., Banerjee, S., Hirano, M., Aizawa, S., Prescott, A. R., and Alessi, D. R. (2010) New roles for the LKB1-NUAK pathway in controlling myosin phosphatase complexes and cell adhesion. *Sci. Signal.* **3,** ra25
8. Hou, X., Liu, J. E., Liu, W., Liu, C. Y., Liu, Z. Y., and Sun, Z. Y. (2011) A new role of NUAK1. Directly phosphorylating p53 and regulating cell proliferation. *Oncogene* **30,** 2933–2942
9. Niesler, C. U., Myburgh, K. H., and Moore, F. (2007) The changing AMPK expression profile in differentiating mouse skeletal muscle myoblast cells helps confer increasing resistance to apoptosis. *Exp. Physiol.* **92,** 207–217
10. Hirano, M., Kiyonari, H., Inoue, A., Furushima, K., Murata, T., Suda, Y., and Aizawa, S. (2006) A new serine/threonine protein kinase, Omphk1, essential to ventral body wall formation. *Dev. Dyn.* **235,** 2229–2237
11. Kusakai, G., Suzuki, A., Ogura, T., Kaminishi, M., and Esumi, H. (2004) Strong association of ARK5 with tumor invasion and metastasis. *J. Exp. Clin. Cancer Res.* **23,** 263–268
12. DeFronzo, R. A., Ferrannini, E., Sato, Y., Felig, P., and Wahren, J. (1981) Synergistic interaction between exercise and insulin on peripheral glucose uptake. *J. Clin. Invest.* **68,** 1468–1474
13. Goodyear, L. J., and Kahn, B. B. (1998) Exercise, glucose transport, and insulin sensitivity. *Annu. Rev. Med.* **49,** 235–261
14. Mu, J., Brozinick, J. T., Jr., Valladares, O., Bucan, M., and Birnbaum, M. J. (2001) A role for AMP-activated protein kinase in contraction- and hypoxia-regulated glucose transport in skeletal muscle. *Mol. Cell* **7,** 1085–1094
15. Jørgensen, S. B., Viollet, B., Andreelli, F., Frøsig, C., Birk, J. B., Schjerling, P., Vaulont, S., Richter, E. A., and Wojtaszewski, J. F. (2004) Knockout of the α2 but not α1 5′-AMP-activated protein kinase isoform abolishes 5-aminoimidazole-4-carboxamide-1-β-4-ribofuranoside but not contraction-induced glucose uptake in skeletal muscle. *J. Biol. Chem.* **279,** 1070–1079
16. Sakamoto, K., Göransson, O., Hardie, D. G., and Alessi, D. R. (2004) Activity of LKB1 and AMPK-related kinases in skeletal muscle. Effects of contraction, phenformin, and AICAR. *Am. J. Physiol. Endocrinol. Metab.* **287,** E310–E317
17. Hayashi, T., Hirshman, M. F., Kurth, E. J., Winder, W. W., and Goodyear, L. J. (1998) Evidence for 5′ AMP-activated protein kinase mediation of the effect of muscle contraction on glucose transport. *Diabetes* **47,** 1369–1373
18. Sakamoto, K., McCarthy, A., Smith, D., Green, K. A., Grahame Hardie, D., Ashworth, A., and Alessi, D. R. (2005) Deficiency of LKB1 in skeletal muscle prevents AMPK activation and glucose uptake during contraction. *EMBO J.* **24,** 1810–1820
19. Fujii, N., Hirshman, M. F., Kane, E. M., Ho, R. C., Peter, L. E., Seifert, M. M., and Goodyear, L. J. (2005) AMP-activated protein kinase α2 activity is not essential for contraction- and hyperosmolarity-induced glucose transport in skeletal muscle. *J. Biol. Chem.* **280,** 39033–39041
20. Koh, H. J., Toyoda, T., Fujii, N., Jung, M. M., Rathod, A., Middelbeek, R. J., Lessard, S. J., Treebak, J. T., Tsuchihara, K., Esumi, H., Richter, E. A., Wojtaszewski, J. F., Hirshman, M. F., and Goodyear, L. J. (2010) Sucrose nonfermenting AMPK-related kinase (SNARK) mediates contraction-stimulated glucose transport in mouse skeletal muscle. *Proc. Natl. Acad. Sci. U.S.A.* **107,** 15541–15546
21. Koh, H. J., Arnolds, D. E., Fujii, N., Tran, T. T., Rogers, M. J., Jessen, N., Li, Y., Liew, C. W., Ho, R. C., Hirshman, M. F., Kulkarni, R. N., Kahn, C. R., and Goodyear, L. J. (2006) Skeletal muscle-selective knockout of LKB1 increases insulin sensitivity, improves glucose homeostasis, and decreases TRB3. *Mol. Cell Biol.* **26,** 8217–8227
22. Fujii, N., Ho, R. C., Manabe, Y., Jessen, N., Toyoda, T., Holland, W. L., Summers, S. A., Hirshman, M. F., and Goodyear, L. J. (2008) Ablation of AMP-activated protein kinase α2 activity exacerbates insulin resistance induced by high-fat feeding of mice. *Diabetes* **57,** 2958–2966
23. Alkhateeb, H., Chabowski, A., Glatz, J. F., Luiken, J. F., and Bonen, A. (2007) Two phases of palmitate-induced insulin resistance in skeletal muscle. Impaired GLUT4 translocation is followed by a reduced GLUT4 intrinsic activity. *Am. J. Physiol. Endocrinol. Metab.* **293,** E783–E793
24. Saito, H., Oda, Y., Sato, T., Kuromitsu, J., and Ishihama, Y. (2006) Multiplexed two-dimensional liquid chromatography for MALDI and nano-electrospray ionization mass spectrometry in proteomics. *J. Proteome Res.* **5,** 1803–1807
25. Rappsilber, J., Ishihama, Y., and Mann, M. (2003) Stop and go extraction tips for matrix-assisted laser desorption/ionization, nanoelectrospray, and LC/MS sample pretreatment in proteomics. *Anal. Chem.* **75,** 663–670
26. Boersema, P. J., Raijmakers, R., Lemeer, S., Mohammed, S., and Heck, A. J. (2009) Multiplex peptide stable isotope dimethyl labeling for quantitative proteomics. *Nat. Protoc.* **4,** 484–494
27. Sugiyama, N., Masuda, T., Shinoda, K., Nakamura, A., Tomita, M., and Ishihama, Y. (2007) Phosphopeptide enrichment by aliphatic hydroxy acid-modified metal oxide chromatography for nano-LC-MS/MS in proteomics applications. *Mol. Cell. Proteomics* **6,** 1103–1109
28. Nakagami, H., Sugiyama, N., Mochida, K., Daudi, A., Yoshida, Y., Toyoda, T., Tomita, M., Ishihama, Y., and Shirasu, K. (2010) Large-scale compar-

ative phosphoproteomics identifies conserved phosphorylation sites in plants. *Plant Physiol.* **153,** 1161–1174
29. Mann, M., and Wilm, M. (1994) Error-tolerant identification of peptides in sequence databases by peptide sequence tags. *Anal. Chem.* **66,** 4390–4399
30. Yamamoto, H., Takashima, S., Shintani, Y., Yamazaki, S., Seguchi, O., Nakano, A., Higo, S., Kato, H., Liao, Y., Asano, Y., Minamino, T., Matsumura, Y., Takeda, H., and Kitakaze, M. (2008) Identification of a novel substrate for TNFα-induced kinase NUAK2. *Biochem. Biophys. Res. Commun.* **365,** 541–547
31. Nagase, T., Ishikawa, K., Miyajima, N., Tanaka, A., Kotani, H., Nomura, N., and Ohara, O. (1998) Prediction of the coding sequences of unidentified human genes. IX. The complete sequences of 100 new cDNA clones from brain which can code for large proteins in vitro. *DNA Res.* **5,** 31–39
32. Bassel-Duby, R., and Olson, E. N. (2006) Signaling pathways in skeletal muscle remodeling. *Annu. Rev. Biochem.* **75,** 19–37
33. Lin, J., Wu, H., Tarr, P. T., Zhang, C. Y., Wu, Z., Boss, O., Michael, L. F., Puigserver, P., Isotani, E., Olson, E. N., Lowell, B. B., Bassel-Duby, R., and Spiegelman, B. M. (2002) Transcriptional co-activator PGC-1α drives the formation of slow-twitch muscle fibres. *Nature* **418,** 797–801
34. McGee, S. L., Sparling, D., Olson, A. L., and Hargreaves, M. (2006) Exercise increases MEF2- and GEF DNA-binding activity in human skeletal muscle. *FASEB J.* **20,** 348–349
35. Kim, Y., Tamura, T., Iwashita, S., Tokuyama, K., and Suzuki, M. (1994) Effect of high-fat diet on gene expression of GLUT4 and insulin receptor in soleus muscle. *Biochem. Biophys. Res. Commun.* **202,** 519–526
36. Tsao, T. S., Stenbit, A. E., Factor, S. M., Chen, W., Rossetti, L., and Charron, M. J. (1999) Prevention of insulin resistance and diabetes in mice heterozygous for GLUT4 ablation by transgenic complementation of GLUT4 in skeletal muscle. *Diabetes* **48,** 775–782
37. Treadway, J. L., Hargrove, D. M., Nardone, N. A., McPherson, R. K., Russo, J. F., Milici, A. J., Stukenbrok, H. A., Gibbs, E. M., Stevenson, R. W., and Pessin, J. E. (1994) Enhanced peripheral glucose utilization in transgenic mice expressing the human GLUT4 gene. *J. Biol. Chem.* **269,** 29956–29961
38. Garvey, W. T., Maianu, L., Zhu, J. H., Brechtel-Hook, G., Wallace, P., and Baron, A. D. (1998) Evidence for defects in the trafficking and translocation of GLUT4 glucose transporters in skeletal muscle as a cause of human insulin resistance. *J. Clin. Invest.* **101,** 2377–2386
39. Kramer, H. F., Witczak, C. A., Taylor, E. B., Fujii, N., Hirshman, M. F., and Goodyear, L. J. (2006) AS160 regulates insulin- and contraction-stimulated glucose uptake in mouse skeletal muscle. *J. Biol. Chem.* **281,** 31478–31485
40. Thong, F. S., Bilan, P. J., and Klip, A. (2007) The Rab GTPase-activating protein AS160 integrates Akt, protein kinase C, and AMP-activated protein kinase signals regulating GLUT4 traffic. *Diabetes* **56,** 414–423
41. Li, Y., Soos, T. J., Li, X., Wu, J., Degennaro, M., Sun, X., Littman, D. R., Birnbaum, M. J., and Polakiewicz, R. D. (2004) Protein kinase Cθ inhibits insulin signaling by phosphorylating IRS1 at Ser^{1101}. *J. Biol. Chem.* **279,** 45304–45307
42. Roach, P. J. (1990) Control of glycogen synthase by hierarchal protein phosphorylation. *FASEB J.* **4,** 2961–2968
43. Fiol, C. J., Mahrenholz, A. M., Wang, Y., Roeske, R. W., and Roach, P. J. (1987) Formation of protein kinase recognition sites by covalent modification of the substrate. Molecular mechanism for the synergistic action of casein kinase II and glycogen synthase kinase 3. *J. Biol. Chem.* **262,** 14042–14048
44. Khamzina, L., Veilleux, A., Bergeron, S., and Marette, A. (2005) Increased activation of the mammalian target of rapamycin pathway in liver and skeletal muscle of obese rats. Possible involvement in obesity-linked insulin resistance. *Endocrinology* **146,** 1473–1481
45. Liu, H. Y., Hong, T., Wen, G. B., Han, J., Zuo, D., Liu, Z., and Cao, W. (2009) Increased basal level of Akt-dependent insulin signaling may be responsible for the development of insulin resistance. *Am. J. Physiol. Endocrinol. Metab.* **297,** E898–E906
46. Richardson, J. M., Balon, T. W., Treadway, J. L., and Pessin, J. E. (1991) Differential regulation of glucose transporter activity and expression in red and white skeletal muscle. *J. Biol. Chem.* **266,** 12690–12694
47. Baron, A. D., Brechtel, G., Wallace, P., and Edelman, S. V. (1988) Rates and tissue sites of non-insulin- and insulin-mediated glucose uptake in humans. *Am. J. Physiol.* **255,** E769–E774
48. Lang, C. H. (1992) Rates and tissue sites of noninsulin- and insulin-mediated glucose uptake in diabetic rats. *Proc. Soc. Exp. Biol. Med.* **199,** 81–87
49. Kim, J. K., Fillmore, J. J., Sunshine, M. J., Albrecht, B., Higashimori, T., Kim, D. W., Liu, Z. X., Soos, T. J., Cline, G. W., O'Brien, W. R., Littman, D. R., and Shulman, G. I. (2004) PKC-θ knockout mice are protected from fat-induced insulin resistance. *J. Clin. Invest.* **114,** 823–827
50. Shillabeer, G., Chamoun, C., Hatch, G., and Lau, D. C. (1995) Exogenous triacylglycerol inhibits insulin-stimulated glucose transport in L6 muscle cells *in vitro*. *Biochem. Biophys. Res. Commun.* **207,** 768–774
51. Montell, E., Turini, M., Marotta, M., Roberts, M., Noé, V., Ciudad, C. J., Macé, K., and Gómez-Foix, A. M. (2001) DAG accumulation from saturated fatty acids desensitizes insulin stimulation of glucose uptake in muscle cells. *Am. J. Physiol. Endocrinol. Metab.* **280,** E229–E237
52. Horike, N., Takemori, H., Katoh, Y., Doi, J., Min, L., Asano, T., Sun, X. J., Yamamoto, H., Kasayama, S., Muraoka, M., Nonaka, Y., and Okamoto, M. (2003) Adipose-specific expression, phosphorylation of Ser^{794} in insulin receptor substrate-1, and activation in diabetic animals of salt-inducible kinase-2. *J. Biol. Chem.* **278,** 18440–18447
53. Dale, S., Wilson, W. A., Edelman, A. M., and Hardie, D. G. (1995) Similar substrate recognition motifs for mammalian AMP-activated protein kinase, higher plant HMG-CoA reductase kinase-A, yeast SNF1, and mammalian calmodulin-dependent protein kinase I. *FEBS Lett.* **361,** 191–195
54. Scott, J. W., Norman, D. G., Hawley, S. A., Kontogiannis, L., and Hardie, D. G. (2002) Protein kinase substrate recognition studied using the recombinant catalytic domain of AMP-activated protein kinase and a model substrate. *J. Mol. Biol.* **317,** 309–323
55. Gwinn, D. M., Shackelford, D. B., Egan, D. F., Mihaylova, M. M., Mery, A., Vasquez, D. S., Turk, B. E., and Shaw, R. J. (2008) AMPK phosphorylation of raptor mediates a metabolic checkpoint. *Mol. Cell* **30,** 214–226
56. Qu, X., Seale, J. P., and Donnelly, R. (1999) Tissue and isoform-selective activation of protein kinase C in insulin-resistant obese Zucker rats. Effects of feeding. *J. Endocrinol.* **162,** 207–214
57. Itani, S. I., Pories, W. J., Macdonald, K. G., and Dohm, G. L. (2001) Increased protein kinase Cθ in skeletal muscle of diabetic patients. *Metabolism* **50,** 553–557
58. Griffin, M. E., Marcucci, M. J., Cline, G. W., Bell, K., Barucci, N., Lee, D., Goodyear, L. J., Kraegen, E. W., White, M. F., and Shulman, G. I. (1999) Free fatty acid-induced insulin resistance is associated with activation of protein kinase Cθ and alterations in the insulin signaling cascade. *Diabetes* **48,** 1270–1274
59. Hoppe, P. E., Chau, J., Flanagan, K. A., Reedy, A. R., and Schriefer, L. A. (2010) *Caenorhabditis elegans* unc-82 encodes a serine/threonine kinase important for myosin filament organization in muscle during growth. *Genetics* **184,** 79–90

J. Biochem. 2012;152(2):171–183 doi:10.1093/jb/mvs041

JB THE JOURNAL OF BIOCHEMISTRY

An anticancer agent, pyrvinium pamoate inhibits the NADH–fumarate reductase system—a unique mitochondrial energy metabolism in tumour microenvironments

Received January 20, 2012; accepted March 30, 2012; published online April 23, 2012

Eriko Tomitsuka[1,2,*†], Kiyoshi Kita[2] and Hiroyasu Esumi[1,3]

[1]Cancer Physiology Project, Research Center for Innovative Oncology, National Cancer Center Hospital East, 6-5-1 Kashiwanoha, Kashiwa, Chiba 277-8577; [2]Department of Biomedical Chemistry, Graduate School of Medicine, The University of Tokyo, 7-3-1 Hongo, Bunkyo-ku, Tokyo 113-0033; and [3]National Cancer Center Research Institute, 5-1-1 Tsukiji, Chuo-ku, Tokyo 104-0045, Japan

*Eriko Tomitsuka, Cancer Physiology Project, Research Center for Innovative Oncology, National Cancer Center Hospital East, 6-5-1 Kashiwanoha, Kashiwa, Chiba 277-8577, Japan email: e-tomi@humeco.m.u-tokyo.ac.jp; Tel/Fax: +81-4-7134-8786

†Present address: Eriko Tomitsuka, Department of Human Ecology, Graduate School of Medicine, The University of Tokyo, 7-3-1 Hongo, Bunkyo-ku, Tokyo 113-0033, Japan

Increased glycolysis is the principal explanation for how cancer cells generate energy in the absence of oxygen. However, in actual human tumour microenvironments, hypoxia is often associated with hypoglycemia because of the poor blood supply. Therefore, glycolysis cannot be the sole mechanism for the maintenance of the energy status in cancers. To understand energy metabolism in cancer cells under hypoxia–hypoglycemic conditions mimicking the tumour microenvironments, we examined the NADH–fumarate reductase (NADH–FR) system, which functions in parasites under hypoxic condition, as a candidate mechanism. In human cancer cells (DLD-1, Panc-1 and HepG2) cultured under hypoxic–hypoglycemic conditions, NADH–FR activity, which is composed of the activities of complex I (NADH–ubiquinone reductase) and the reverse reaction of complex II (quinol–FR), increased, whereas NADH-oxidase activity decreased. Pyrvinium pamoate (PP), which is an anthelmintic and has an anti-cancer effect within tumour-mimicking microenvironments, inhibited NADH–FR activities in both parasites and mammalian mitochondria. Moreover, PP increased the activity of complex II (succinate–ubiquinone reductase) in mitochondria from human cancer cells cultured under normoxia–normoglycemic conditions but not under hypoxia–hypoglycemic conditions. These results indicate that the NADH–FR system may be important for maintaining mitochondrial energy production in tumour microenvironments and suggest its potential use as a novel therapeutic target.

Keywords: complex I/complex II/NADH–fumarate reductase system/pyrvinium pamoate/tumour microenvironments.

Abbreviations: $\Delta\Psi m$, mitochondrial membrane potential; ETC, electron transport chain; NADH–FR, NADH–fumarate reductase; NADH–RQR, NADH–rhodoquinone reductase; NADH–UQR, NADH–ubiquinone reductase; PA, pamoic acid; PP, pyrvinium pamoate; QFR, quinol–fumarate reductase; SDH, succinate dehydrogenase; SQR, succinate–ubiquinone reductase; UQ, ubiquinone.

When adequate oxygen is supplied to tissue, ATP is mainly generated by oxidative phosphorylation through the electron transport chain (ETC) in the mitochondria of most human tissues. In normal tissues, the oxygen concentration is well maintained by physiological responses. In tumour tissues, on the other hand, the oxygen concentration is known to be heterogeneous both topologically and temporally and in general is relatively and sometimes extremely low (*1*, *2*). Moreover, in hypovascular tumours, such as pancreatic cancer, the deprivation of both oxygen and nutrients occurs as a result of the limited blood supply to the tumour tissues. Reportedly, the glucose concentration is markedly lower in tumour tissues than in normal tissues (*3*). However, cancer cells are known to obtain energy mainly by glycolysis, as observed by the increase in glucose uptake and lactate production, known as the Warburg effect (*4*). As some cancer cells do not show a high activity of glycolysis (*5*) and the quantity of glucose is restricted in hypovascular tumours, Warburg effect alone cannot explain how cancer cells sustain their required energy levels under such conditions.

When tumour microenvironments are mimicked by the withdrawal of nutrients and oxygen, cancer cells become resistant to conventional chemotherapeutics. Lu *et al.* (*6*) have shown that traditional anticancer agents, such as 5-FU and cisplatin, exhibit cytotoxicity in normal medium but only minimal effects in nutrient-free medium. Under hypoxic condition, cancer cells have been shown to become resistant to some anticancer agents, such as bleomycin and vincristine (*7*). The molecular mechanism for hypoxia-induced drug resistance is not well understood, but the development of anticancer agents effective under nutrient-starved and hypoxic conditions or even specifically effective under such conditions is mandatory (*8*).

In this regard, we have reported on several anticancer agents that exert cytotoxic effects selectively

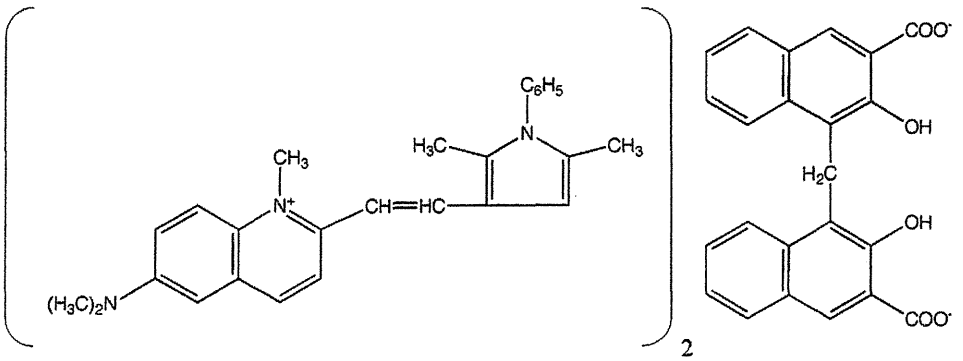

Fig. 1 Structural formula for pyrvinium pamoate.

under nutrient-depleted conditions mimicking tumour microenvironments. Kigamicin D and arctigenin are highly cytotoxic in nutrient-free medium and exhibit antitumour activities (*6*, *9*). Pyrvinium pamoate (PP; Fig. 1), an anthelmintic also showed an anti-cancer activity against human cancer cells (*10*). Parasitic helminths live in the intestines of their mammalian hosts, where the oxygen concentration is relatively low and they use the phosphoenolpyruvate carboxykinase (PEPCK)-succinate pathway for hypoxic energy production. The final step in this pathway is the NADH–fumarate reductase (NADH–FR) system (*11*). PP is considered an effective and useful anthelmintic for pinworm infections when administered orally and a single dose of 5 mg per kg body weight in adult humans is highly effective (*12*). The inhibitory effect of PP on pinworms is thought to occur as a result of interference with glucose absorption in parasites (*13*). In addition, the mechanism responsible for the inhibitory effect of PP is thought to result from the inhibition of mitochondrial fumarate reductase (FRD) activity (*13*). Recently, PP has been shown to exhibit anti-parasitic activities against some parasite infections, such as cryptosporidiosis and malaria (*14*, *15*), as well as an anticancer-effect on human cancer cell xenografts (*10*, *16*, *17*). However, the mechanisms of these effects have not been fully elucidated. In human cultured cells, PP also showed some pharmacological effects, including the inhibition of androgen receptors and the dependent gene transcription inhibition of ER stress, leading to cell death (*18*).

In this report, at first, to clarify the function of ETC in tumour microenvironments, activity changes in normoxic and hypoxic ETCs were compared. Next, to clarify the mechanisms of the anti-parasitic and anti-cancer effects of PP in parasites and mammals, respectively, the effects on enzyme activities in the ETC of helminths and mammals were examined. Thirdly, to understand how and why PP exhibits an anticancer activity specifically within tumour microenvironments, the effects of PP on mitochondrial energy metabolism under normal and tumour-microenvironment-mimicking conditions were compared. Finally, we investigated the mechanism of the action of PP on one of the mitochondrial ETC enzymes, complex II.

Materials and Methods

Materials

PP, pamoic acid (PA), ubiquinone-1 and ubiquinone-2 were purchased from Sigma. Sucrose monolaurate was purchased from Iwai Chemicals. Decyl-rhodoquinone was synthesized as described (*19*). All other chemicals were purchased from Wako and Sigma.

Cell culture

Human pancreatic cancer cells (Panc-1) and human hepatocellular carcinoma cells (HepG2) were cultured in DMEM (GIBCO BRL), human colorectal adenocarcinoma cells (DLD-1) were cultured in RPMI-1640 (GIBCO BRL) and human dermal fibroblast cells (HDF: TOYOBO) were cultured in DMEM/F12 (GIBCO BRL) supplemented with 10% heat-inactivated foetal bovine serum (Tissue Culture Biochemicals) and antibiotics in 75 cm^2 tissue culture flasks (CORNING) under 5% CO_2 at 37°C. All the cells except for HDF were purchased from ATCC. All cells were maintained under normal conditions. After 3 days, the medium was changed for glucose depleted, glucose and glutamine-free DMEM (Sigma) with 10% heat-inactivated dialysed foetal bovine serum, and for hypoxia, the cells were cultured in an atmosphere of 5% CO_2, 1% O_2 and 94% N_2 at 37°C. To collect all cells, detaching cells were trypsinized and floating cells in cultured medium were centrifuged and all cells were counted with a Cell Countess™ automated cell counter according to the manufacturer's protocol (Invitrogen). Viable cells and dead cells were identified by dye-exclusion with trypan blue.

Preparation of mitochondria

Mitochondria were prepared from cultured cells as described previously (*20*). The mitochondrial proteins were solubilized with 2.5% (w/v) sucrose monolaurate, 1/100 volume of protease inhibitor cocktail (Sigma), 1 mM sodium malonate and 1/100 volume of phosphatase inhibitors I and II (Sigma) and were stirred on ice for 1 h. After centrifugation at 72,000 × *g* for 20 min at 4°C, the supernatant was subjected to 2D gel electrophoresis or phosphatase treatment.

Ascaris suum mitochondria were prepared from the muscle of adult *A. suum* as described previously (*21*). Bovine submitochondrial particles were prepared from bovine heart as described previously (*22*).

The protein concentrations were estimated using the Bradford method (*23*).

Enzyme assays

The mitochondrial activities of succinate dehydrogenase (SDH) (*24*), succinate ubiquinone reductase (SQR) (*25*), quinol–fumarate reductase (QFR), NADH–FR, NADH–ubiquinone reductase (NADH–UQR) and NADH–rhodoquinone reductase (NADH–RQR) (*25*, *26*) were assayed as described previously. All the assays were performed at 25°C except for the NADH–FR assay (performed at 30°C) using 50 mM potassium phosphate (pH 7.5) as a reaction buffer. PP and PA were incubated with mitochondrial samples in a reaction buffer for 5 min at 25°C before the addition of the substrate.

Measurement of mitochondrial oxygen consumption

Mitochondrial oxygen consumption was measured using a Biological Oxygen Monitor 5300 (Yellow Spring Instrument) with

Clark type oxygen electrodes (*27*). Potassium phosphate (50 mM, pH 7.5) was used as a reaction buffer. Bovine submitochondrial particles (100 μg/mL) and PP were added and the reaction was started by the addition of 5 mM of potassium succinate or 1 mM of NADH as a substrate.

2D polyacrylamide gel electrophoresis

2D gel electrophoresis was performed as described previously (*20*). Solubilized mitochondrial proteins and 9.2 M urea, 1% (w/v) sucrose monolaurate, 0.6% (w/v) DTT, 2% (v/v) IPG buffer, a small amount of Orange G and a pI marker (BDH; Range 5.65 ~ 8.3) were added and run on an IPGphor isoelectric focusing unit (GE Healthcare) according to the manufacturer's protocol. For the second dimension, the strips were equilibrated with SDS–PAGE running buffer for 5 min at room temperature and then applied to 12.5% polyacrylamide gels and analysed using immunoblotting.

Treatment with phosphatase

For the phosphatase treatment, the solubilized mitochondrial proteins in Antarctic Phosphatase buffer containing protease inhibitor cocktails were treated with Antarctic Phosphatase (BioLabs) at 37°C for 2 h. For the phosphatase treatment negative control, 1/100 volumes of phosphatase inhibitors I and II were added (*20*).

Measurement of mitochondrial membrane potentials

Freshly prepared mitochondria were suspended at a concentration of 1 mg protein/mL in 220 mM sucrose, 68 mM mannitol, 10 mM potassium chloride, 5 mM KH_2O_4, 2 mM $MgCl_2$, 0.5 mM EGTA and 10 mM HEPES (pH 7.4). One hundred microlitres of the samples was poured on a 96-well plate and 5 μM of Rhodamine 123 was added. The fluorescence emission was monitored at room temperature using 538 nm as the emission wavelength and 485 nm as the excitation wavelength for 5 min (10 counts/min) in Asent Fluoroskan (Labsystem). Mitochondrial membrane potential ($\Delta\Psi m$) build-up was stimulated by the addition of 1 mM sodium succinate or 1 mM sodium fumarate as a substrate and incubated for 5 min, then measured for 5 min. Sodium cyanide (10 mM) was added as the inhibitor of complex IV, 0.5 μM PP was added after the addition of the substrates and the samples were incubated and measured for 5 min each. Finally, 100 nM of carbonyl cyanide-*p*-trifluoromethoxyphenylhydrazone (FCCP), a mitochondrial uncoupling reagent, was added to collapse the formed membrane potential (*28*). The membrane potentials were calculated based on the values for Rhodamine 123 fluorescence quenching as determined by the Rhodamine 123 fluorescence in a sample that did not contain mitochondria.

Statistical analysis

Data from the two experimental groups were compared using the Student's *t*-test. Statistical significance was defined as $P < 0.05$.

Results

Changed ETC enzyme activities and effect of PP in tumour microenvironments in human cancer cells

In hypovascular tumours, both the deprivation of oxygen and glucose were observed, because of the limitation of the blood supply to the tumour tissues. We wondered whether human cancer cells survive under hypoxia–hypoglycemic conditions mimicking tumour microenvironments. Such conditions have been reported in the short term. When HepG2 cells were cultured for 36 h under the depletion of both oxygen and glucose, *i.e.* hypoxia–hypoglycemic conditions, cells survived whereas they died under glucose starvation in normoxia (*29*). To confirm cancer cells can survive under microenvironments mimicking tumour conditions in the long term, cells were cultured in glucose-depleted medium under hypoxic conditions for 1 week. In DLD-1, under hypoxia–hypoglycemic conditions, 73.8% cells survived for 7 days (Fig. 2).

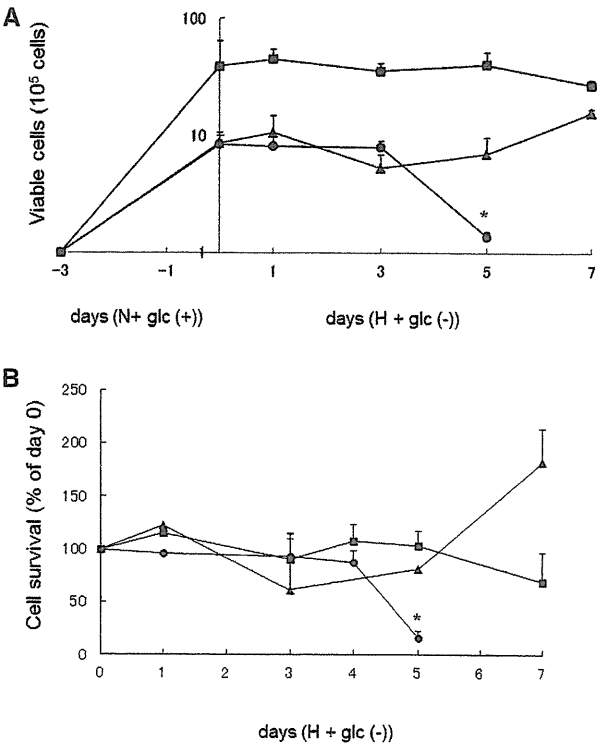

Fig. 2 Cell survivals under hypoxia–hypoglycemic conditions. (**A**) Number of surviving cells. (**B**) The percentages of cell survival from day 0. The circles indicate HDF, the squares indicate DLD-1 and the triangles indicate Panc-1 cultured under 1% O_2 and glucose depleted conditions [H+ glc(−)] for 1–7 days. All the data were expressed as the mean ± SEM of three independent measurements. Statistically significant differences with respect to day 0 are shown by an asterisk (Student's *t*-test).

Panc-1 also survived under such conditions for 7 days. On the other hand, cell survival rate was decreased in 16.3% of HDF by day 5. Thus, human cancer cells can survive under hypoxia–hypoglycemic conditions for the long term. This result is consistent with the fact that cancer cells in tumour tissues can survive under tumour microenvironments.

In a previous report, activities of the reverse reaction of complex II, which is the component of NADH–FR system, were found in all six human cancer cell lines examined including DLD-1, Panc-1 and HepG2 (*20*), suggesting that the NADH–FR system can be enabled in cancer cells and NADH–FR activities were detected in all the cell cultures in our experiment (data not shown). Then to examine whether the ETC function changes from normoxic ETC to hypoxic ETC; NADH-oxidase [Fig. 3A(a)] and NADH–FR [Fig. 3A(b)] activities were measured. In DLD-1 cultured under hypoxia–hypoglycemic conditions, NADH-oxidase activity eventually decreased to an undetectable level, whereas NADH–FR activity was 3.0 ± 0.4 nmol/min/mg mitochondrial proteins under normoxia–normoglycemic conditions and 10.4 ± 1.0 nmol/min/mg proteins after 7 days of hypoxia–hypoglycemic conditions [Fig. 3B(a)]. Other cancer cell lines, Panc-1 and HepG2, also showed the same response, *i.e.* a decrease in NADH-oxidase activity, whereas an increase in NADH–FR activity was

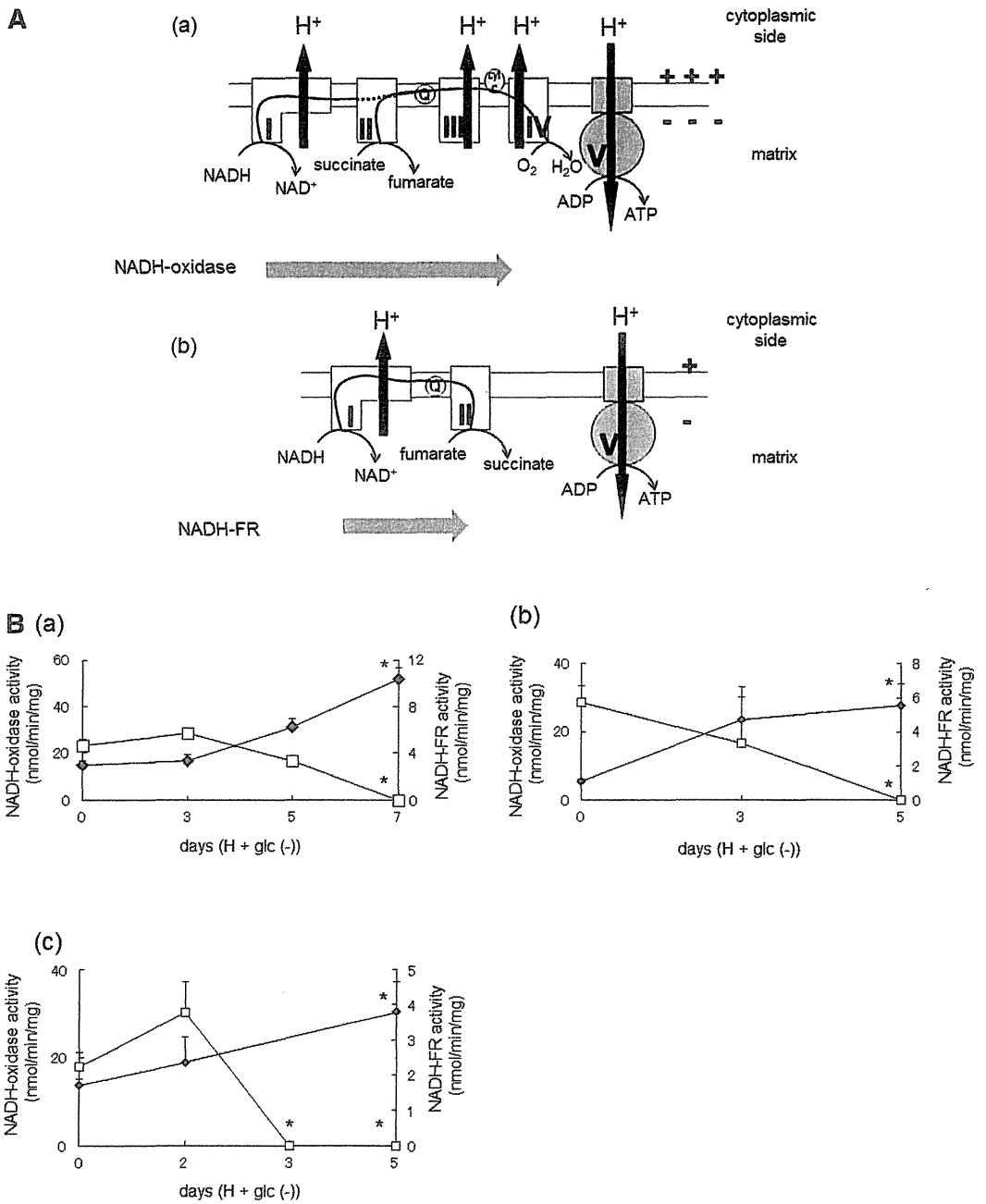

Fig. 3 Electron transport chain enzyme activities in mitochondria. (A) Mitochondrial respiratory chains. (**a**) Oxidative phosphorylation system. Under normoxic conditions in mammalian mitochondria, electrons from the TCA cycle pass through complex I (I: NADH–ubiquinone reductase) to ubiquinone (Q), complex III (III: ubiquinol–cytochrome *c* reductase), cytochrome *c* (cyt *c*) and complex IV (IV: cytochrome *c* oxidase) or through complex II (II: succinate–ubiquinone reductase) to ubiquinone, complex III, cytochrome *c* and complex IV. At the same time, complex I, complex III and complex IV function as proton pumps to generate a proton gradient, driving complex V (ATP synthase). (**b**) NADH–FR system. Under hypoxic conditions, electrons pass through complex I and the reverse reaction of complex II (FRD). Only complex I functions as a proton pump, generating a proton gradient and driving complex V even in the absence of oxygen. (**B**) Mitochondrial ETC enzyme activities from DLD-1 (**a**), Panc-1 (**b**) and HepG2 (**c**) cultured under 1% O_2 and glucose depleted conditions [H+ glc(−)]. The open squares indicate the NADH-oxidase activities (complex I–III–IV). The closed diamonds indicate the NADH–FR activities (complex I–II). All the data were expressed as the mean ± SEM of three independent measurements. Statistically significant differences with respect to day 0 are shown by an asterisk (Student's *t*-test).

observed under hypoxia–hypoglycemic conditions [Fig. 3B(b,c)]. When the Panc-1 mitochondrial proteins were separated using blue native gel electrophoresis (BN–PAGE), which can separate ETC enzyme complexes according to native forms, the complex I activity per subunit protein (NDUFSA3) was found to remain at almost the same levels under hypoxia–hypoglycemic conditions [Supplementary Fig. S1C(a)]. However, SDH activities decreased under hypoxia–hypoglycemic conditions and even the iron–sulphur protein (Ip) subunit proteins of complex II were detected at the same levels indicating that protein levels of complex II unchanged under such conditions [Supplementary Figs. S1A(b) and S1B(b)]. Complex

IV activities per subunit proteins also decreased under hypoxia–hypoglycemic conditions [Supplementary Fig. S1C(c)]. Moreover, a low molecular weight complex IV subunit, COXI, protein was detected, suggesting the degradation of complex IV [Supplementary Fig. S1B(d)]. These data are consistent with the changes in enzyme activities and the levels of proteins making up the ETC complexes. Complex I changed minimally, both in its activity and its protein level, because complex I contributes to both normoxic and hypoxic ETCs, whereas complexes of normoxic ETC such as complex IV, decreased in their activities and protein levels under conditions mimicking tumour microenvironments.

PP was selectively cytotoxic to human cancer cells cultured in a nutrient-free medium mimicking the tumour microenvironment (*10*). We investigated whether PP shows cytotoxic effect in human cells, cancer cells and normal cells under normoxia–normoglycemic and hypoxia–hypoglycemic conditions. PP showed a cytotoxic effect for cancer cells, DLD-1 and Panc-1, under hypoxia–hypoglycemic conditions, whereas little cytotoxic effect was observed under normoxia–normoglycemic conditions (Fig. 4). Moreover, PP exerted minimal cytotoxicity on normal fibroblast (HDF) cells under either normoxia–normoglycemic or hypoxia–hypoglycemic conditions (Fig. 4).

Effect of PP on enzyme activities in normoxic and hypoxic ETCs

PP is used as an anthelmintic and is believed to inhibit fumarate respiration in parasitic energy metabolism, although no direct data or evidence has been reported. To confirm the effect of PP on ETC in parasitic and mammalian mitochondria, we measured the enzyme activities of ETC enzymes in adult *A. suum* and bovine heart mitochondria. The activities of hypoxic ETC enzymes such as NADH–FR, NADH–RQR and QFR, all of which are components of the NADH–FR system, were higher in adult *A. suum* mitochondria than in bovine mitochondria (Table I). These results were consistent with the conclusion that adult *A. suum* uses the NADH–FR system for hypoxic energy metabolism. PP inhibited NADH–RQR, NADH–UQR (complex I) and QFR (complex II) activities, with an IC_{50} of 0.3 μM for NADH–RQR, 33 μM for NADH–UQR and 9.5 μM for QFR in adult *A. suum* mitochondria. For NADH–FR, which is defined as hypoxic complex I and complex II activities, the IC_{50} was 0.5 μM in *A. suum*. The complex II activities, SQR and SDH, both decreased with 50 μM of PP and 50 μM of PA to the same levels in *A. suum* mitochondria. These data suggest that the inhibitory effects on SQR and SDH in *A. suum* were caused by PA and not pyrvinium itself. The minimal side effects of PP are reportedly due to the non-absorption of PP by the gastrointestinal tract in humans (*12*). However, another pyrvinium salt, pyrvinium chloride, has been reported to be selectively toxic in rodents because of its absorption only in rodent species (*30*). These reports indicate that the salt types of PP have different effects in mammals.

In bovine heart mitochondria, PP inhibited the NADH–UQR (complex I) and the IC_{50} was 0.7 μM (Table I). PP inhibited QFR in bovine heart mitochondria and the IC_{50} was 14 μM (similar to the level for QFR in *A. suum*), but no inhibitory effects on SQR and SDH were seen. Of note, incubation with 50 μM of PP increased the SQR activity by approximately 150%, whereas PA had no effect on the SQR or SDH activities. These effects of PP on SQR were quite different between *A. suum* and bovine mitochondria.

To confirm the effects of PP on the mammalian ETC overall, the oxygen consumption by bovine mitochondria was measured. As shown in Fig. 5, the reaction started by the addition of succinate, representing the succinate oxidase activity, gradually increased

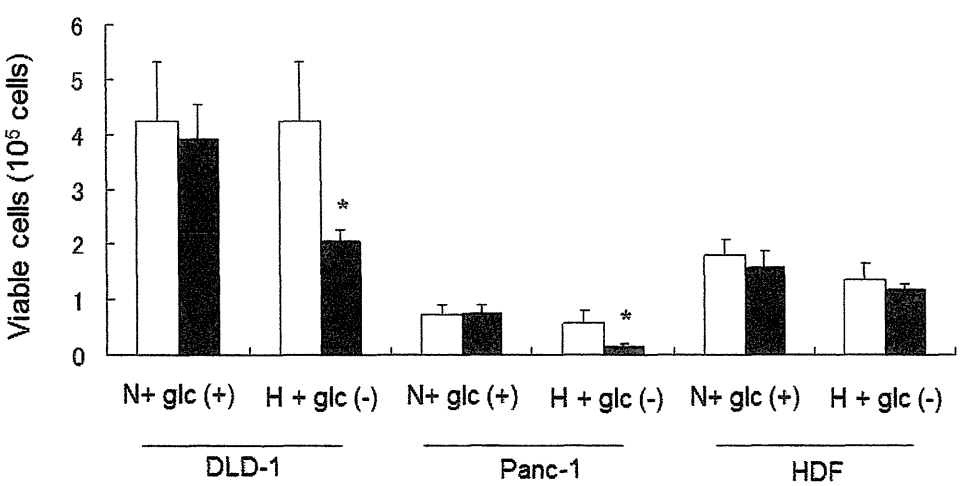

Fig. 4 Cytotoxicity of pyrvinium pamoate in DLD-1, Panc-1 and HDF under normoxia–normoglycemic and hypoxia–hypoglycemic conditions. Cells were cultured in normoglycemic medium at atmospheric oxygen tension [N+ glc(+)] for 3 days and treated with PP (0.1 μM) in N+ glc(+) or glucose-free medium under 1% oxygen [H+ gluc(−)] for 24 h. The open bars indicate the number of viable cells after treatment with DMSO, whereas the closed bars indicate the number of viable cells after treatment with PP. The values reported represent the mean ± SEM of three independent measurements. Statistically significant differences with respect to the control (DMSO treated) are shown by an asterisk (Student's *t*-test).

Table I. Enzyme activities of electron transport chain enzymes and the effects of pyrvinium pamoate and pamoic acid.

	Enzyme activity (nmol/min mg protein)	PP IC_{50} (μM)	Residual activity of 50 μM PP (%)	Residual activity of 50 μM PA (%)
Adult *Ascaris suum* mitochondria				
Complex I + II (NADH–FR)	51.7 ± 8.3	0.5	n.d.	99.4
Complex I (NADH–UQR)	110.3 ± 7.4	33.0	n.d.	102.4
Complex I (NADH–RQR)	65.0 ± 1.7	0.3	n.d.	107.8
Complex II (QFR)	42.2 ± 5.4	9.5	n.d.	105.3
Complex II (SQR)	268.7 ± 24.4	No inhibition	61.7	47.9
Complex II (SDH)	182.4 ± 2.1	No inhibition	59.9	69.5
Bovine heart submitochondrial particles				
Complex I + II (NADH–FR)	8.5 ± 1.9	0.5	n.d.	94.8
Complex I (NADH–UQR)	139.5 ± 33.5	0.7	n.d.	93.3
Complex I (NADH–RQR)	13.4 ± 1.7	2.9	n.d.	n.d.
Complex II (QFR)	6.6 ± 0.3	14.0	n.d.	n.d.
Complex II (SQR)	65.3 ± 10.1	No inhibition	154.2	93.9
Complex II (SDH)	37.2 ± 12.3	No inhibition	100.0	93.0

NADH–FR, NADH–fumarate reductase; NADH–UQR, NADH–ubiquinone reductase; NADH–RQR, NADH–rhodoquinone reductase; QFR, Rhodoquinol–fumarate reductase; SQR, succinate–ubiquinone reductase; SDH, succinate dehydrogenase. n.d., not done.

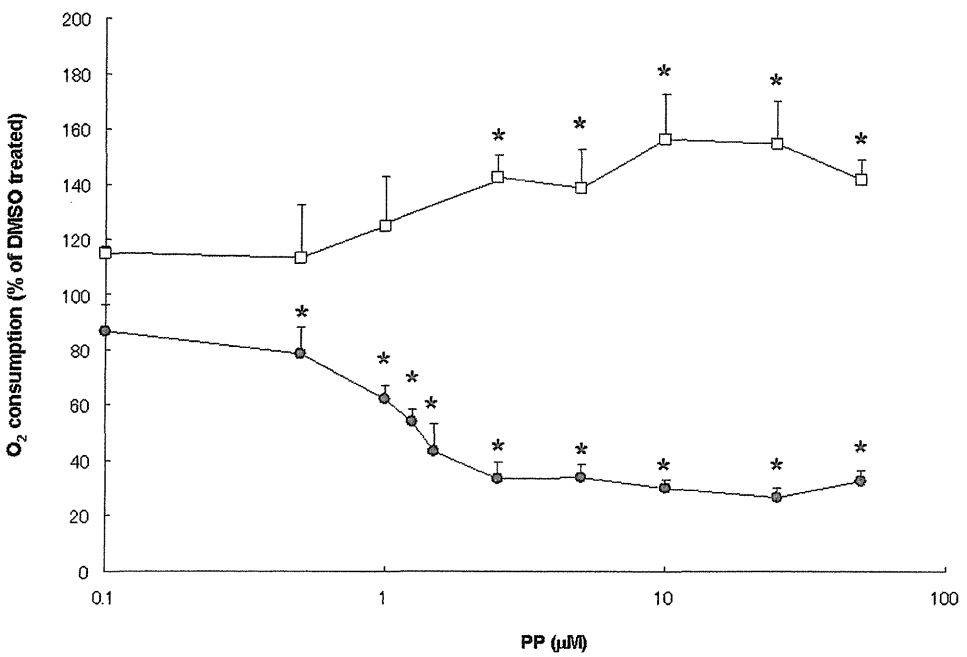

Fig. 5 Effects of pyrvinium pamoate on oxygen consumption in bovine mitochondria. The open squares indicate the percentages of residual activity using succinate as the substrate and the closed circles indicate the percentages of residual activity using NADH as the substrate. The oxygen consumption rate without PP was defined as 100%. The values reported represent the mean ± SEM of three independent measurements. Statistically significant differences with respect to the control (DMSO treated) are shown by an asterisk (Student's *t*-test).

with the addition of PP, whereas the reaction started by the addition of NADH, representing the NADH-oxidase activity, decreased, although the activity remained at 20% for a high dose of PP. These data are consistent with the data in Table I, showing an increase in SQR activity and the partial inhibition of NADH–UQR activity.

Effect of PP on normoxic and hypoxic ETC enzymes and on mitochondrial functions under hypoxia–hypoglycemic conditions

PP inhibited the enzymatic activities in the NADH–FR system in mammalian mitochondria but did not inhibit SQR or SDH, as shown in Table I. These observations implied that PP has different effects on the ETC enzymes of cancer cells under hypoxia–hypoglycemic conditions, compared with under normoxia–normoglycemic conditions. To confirm whether PP exerts different effects on SQR and NADH–FR activities in cancer cells in tumour microenvironments, we measured these activities in mitochondria from cancer cells cultured under hypoxia–hypoglycemic conditions for 3 and 5 days (7 days in DLD-1). Under normoxia–normoglycemic conditions on day 0, PP increased the SQR activity in both Panc-1 and DLD-1 mitochondria as well as in bovine mitochondria (Fig. 6A). However, after the cells had been cultured under hypoxia–hypoglycemic

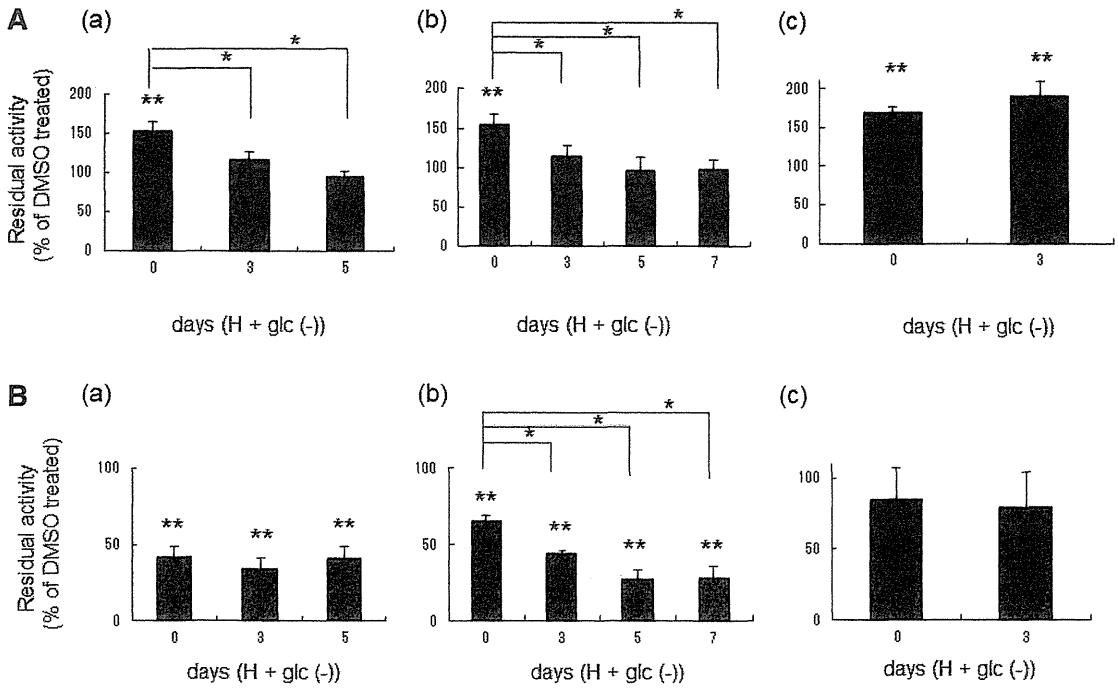

Fig. 6 Effects of pyrvinium pamoate on SQR and NADH–FR activities under hypoxia–hypoglycemic conditions. (**A**) Effect of 25 μM PP on SQR activity. The percentages of the residual SQR activities from the addition of DMSO instead of PP in mitochondria separated from Panc-1 (**a**), DLD-1 (**b**) and HDF (**c**) cultured under normoxia–normoglycemic conditions [N+ glc (+)] (day 0) and cultured in glucose-free medium under 1% O_2 [H+ glc (−)] [days 3 and 5 (and 7 in DLD-1)] are shown. (**B**) Effect of 5 μM PP on NADH–FR activity. The percentages of the residual NADH–FR activities in mitochondria separated from Panc-1 (**a**), DLD-1 (**b**) and HDF (**c**) cultured under N+ glc (+) (day 0) and cultured under H+ glc(−) [days 3 and 5 (and 7 in DLD-1)] are shown. The values reported represent the mean ± SEM of three independent measurements. Statistically significant differences are shown by the asterisks (*$P<0.05$ versus day 0, **$P<0.05$ versus DMSO treated, Student's *t*-test).

conditions for 3–5 days (7 days in DLD-1), PP no longer had any activation effect on SQR [Fig. 6A(a,b)]. When HDF was cultured under the same hypoxic–hypoglycemic conditions, PP increased the SQR activity in a manner similar to that under normoxia–normoglycemic conditions [Fig. 6A(c)]. On the other hand, the NADH–FR activities in Panc-1 and DLD-1 mitochondria were inhibited by PP under both conditions, but an inhibitory effect was not evident in HDF, partly because of the low NADH–FR activity of HDF [Fig. 6B(c)]. Interestingly, in DLD-1, the inhibitory effect on NADH–FR activity gradually increased over time when the cells were cultured under hypoxia–hypoglycemic conditions [Fig. 6B(b)]. PP also inhibited NADH–UQR activity as shown in Table I and the effect of PP on NADH–UQR in mitochondria from cultured cells was also compared (Supplementary Fig. S2). PP inhibited NADH–UQR activities under both normoxia–normoglycemic and hypoxia–hypoglycemic conditions in all cell lines including HDF, but the inhibitory effect in HDF was smaller than that in other cancer cell lines. In mitochondria prepared from cancer cells cultured under hypoxia–hypoglycemic conditions, the increase in SQR activity induced by PP disappeared, whereas the reverse reaction of complex II in the NADH–FR system was inhibited by PP. In contrast, under both normoxia–normoglycemic and hypoxia–hypoglycemic conditions, minimal differences in the inhibitory effects of NADH–UQR were observed. The distinct effects of PP on complex II activities may be one of the reasons why PP is only cytotoxic in cancer cells within tumour microenvironments but does not exhibit cytotoxicity in normal cells or cancer cells within normoxia–normoglycemic environments.

As PP affected both normoxic and hypoxic ETC in mitochondria, we examined the effects of PP on the mitochondrial membrane potential ($\Delta\Psi m$) to confirm how PP affects mitochondrial functions in cancer cells. In normoxic ETC, electrons from the TCA cycle pass via complex I (NADH–UQR) → complex III (ubiquinol–cytochrome *c* reductase) → complex IV (cytochrome *c* oxidase) or via complex II (SQR) → complex III → complex IV. Complex I, complex III and complex IV function as proton pumps and generate a proton gradient, which is the driving force for ATP synthesis by complex V (ATP synthase) as shown in Fig. 3A(a). On the other hand, the NADH–FR system is only composed of complex I and the reverse reaction of complex II; thus, only complex I functions as a proton pump, forming a transmembrane electrochemical proton gradient for ATP synthesis through complex V [Fig. 3A(b)]. The generation of a $\Delta\Psi m$ indicates that the ETC enzymes are actively functioning as proton pumps. If PP affects the $\Delta\Psi m$, the generation of ATP will be influenced. To understand whether and how the NADH–FR system can generate a $\Delta\Psi m$, fumarate was first used as the substrate of the NADH–FR system and the generation of a $\Delta\Psi m$ in mitochondria prepared from cancer cells cultured under

normoxia–normoglycemic or hypoxia–hypoglycemic conditions was measured. Because a $\Delta\Psi m$ was generated using the NADH–FR system and both fumarate and NADH as substrates, fumarate was used as a substrate for the generation of $\Delta\Psi m$ in the presence of endogenous NADH. When mitochondria prepared from cells cultured under normoxia–normoglycemic conditions were used, as shown in Fig. 7A(a), $\Delta\Psi m$ was increased by the addition of succinate. The $\Delta\Psi m$ generated by succinate was inhibited by 0.1 mM of cyanide [Fig. 7A(a)]. Cyanide did not inhibit the $\Delta\Psi m$ generated by fumarate, as shown in Fig. 7A(b). As the NADH–FR system is composed of complex I and complex II, and complex IV is not included in this system, the finding that the $\Delta\Psi m$ generated by fumarate was insensitive to cyanide is consistent with the idea that cancer cells utilize the NADH–FR system. As shown in Fig. 7B and C, 0.5 μM of PP inhibited the $\Delta\Psi m$ generated by fumarate in Panc-1 and DLD-1. No inhibitory effect of PP was observed on the $\Delta\Psi m$ generated by succinate in Panc-1 [Fig. 7B(a)]. Moreover, in DLD-1, PP slightly but reproducibly increased the $\Delta\Psi m$ generated by succinate [Fig. 7C(c)]. A similar effect of PP on the $\Delta\Psi m$ generated by succinate was observed in HepG2 cells (data not shown). These data coincided with the data in Fig. 6 and PP increased the activity of SQR under normoxia–normoglycemic conditions.

Effect of PP on the Fp subunit in complex II

As PP increased the activity of SQR (Table I, Figs 5 and 6), the effect of PP on human complex II was examined. Previously, we reported that the enzyme activities of human complex II are regulated by the phosphorylation of the flavoprotein (Fp) subunit, which is the catalytic subunit of complex II (*20*). In our previous paper, treatment with a phosphatase caused the dephosphorylation of the Fp subunit and an increase in the SQR activity, whereas the reverse reaction of complex II, *i.e.* fumarate reductase (FRD) activity were decreased in DLD-1 mitochondria. In contrast, treatment with protein kinase caused the phosphorylation of the Fp subunit and a decrease in SQR activity with a concomitant increase in FRD activity. As mentioned, treatment with PP resulted in an increase in SQR activity and we suspected that PP treatment may modulate the phosphorylation of the Fp subunit of complex II. In Fig. 8A, treatment with phosphatase increased the SQR activity in DLD-1 mitochondria and PP also increased the SQR activity, relative to a control (0 U of Antarctic phosphatase treatment). Moreover, treatment with PP plus phosphatase exerted a stronger activation effect on SQR. However, 2 U of phosphatase treatment produced the same activation effect as PP plus phosphatase, suggesting that a high amount of phosphatase can cause the complete dephosphorylation of the Fp subunit related to SQR activity. Therefore, PP has the same effect as phosphatase on SQR activity.

Next, to determine whether PP causes the dephosphorylation of the Fp subunit in a manner similar to phosphatase treatment, the phosphorylation status of the Fp subunit was examined. In Fig. 8B, Fp protein spots with different pI values were detected and the spot intensities differed for each treatment. The ratios of the intensity of spot No.3 to the intensity of spot No.4 were increased after PP treatment, indicating that the ratio of dephosphorylated Fp proteins increased (Fig. 8C). These data suggest that PP causes the dephosphorylation of Fp leading to an increase in SQR activity and the effect of PP might be related to mitochondrial phosphatases. To address the question of whether the effect of PP arises from the activation of phosphatase, PP was treated with phosphatase inhibitors. In Fig. 9A, PP increased the SQR activity, whereas treatment with PP and phosphatase inhibitors did not produce any increase in SQR activity. Similarly, the treatment with phosphatase increased the SQR activity, whereas the treatment with phosphatase together with phosphatase inhibitors did not increase the SQR activity (Fig. 9B). These data suggest that PP affects the complex II activity indirectly, indicating that PP enhances SQR activity through the activation of mitochondrial phosphatase(s).

Discussion

In this report, we investigated the existence and function of the hypoxic ETC, the NADH–FR system, in tumour microenvironments in human cancer cells and the mechanisms of the effects of PP on parasitic and mammalian ETC enzymes. PP inhibited the hypoxic ETC, NADH–FR system in both parasitic and mammalian mitochondria, showing that the NADH–FR system is active in both parasitic and mammalian mitochondria. Moreover, PP inhibited SQR activity in parasitic mitochondria but activated SQR activity in mammalian mitochondria. The species-specific effect of PP is likely caused by the distinct function of complex II in mammalian mitochondria. We also showed that PP had different effects on complex II activities in cancer cells cultured under normoxic–normoglycemic conditions and under hypoxic–hypoglycemic conditions, suggesting that treatment with PP may be selectively effective against cancer cells in tumour microenvironments. In addition, we showed that PP dephosphorylated the Fp subunit in complex II and activated SQR activity, similar to the effect of phosphatase, indicating that PP activates mitochondrial protein phosphatases that maintain the functions of ETCs.

Recently, PP has been shown to exert not only anti-pinworm but also anti-malarial and anti-cryptosporidium activities (*14*, *15*). The search for anti-parasitic drugs is continuing in the 21st century and pathways of parasitic energy metabolism, such as the NADH–FR system, are gradually becoming viewed as important candidate targets for anti-parasitic drugs (*31*, *32*). In our study we found that PP inhibited the NADH–FR system, consisting of both complex I and complex II activities, in *A. suum* mitochondria, suggesting that PP kills these parasites by inhibiting the NADH–FR system. Therefore, this system may be important for energy production in parasites and may be a useful target